Evolutionary Dynamics Under Various Modes of Reproduction

Jacob Devin Cooper

A dissertation

submitted in partial fulfillment of the

requirements for the degree of

Doctor of Philosophy

University of Washington

2016

Reading Committee:

Benjamin Kerr, Chair

Carl T Bergstrom, Chair

Toby Bradshaw

Program Authorized to Offer Degree:

Biology

University of Washington

Abstract

Evolutionary Dynamics Under Various Modes of Reproduction

Jacob Devin Cooper

Chairs of the Supervisory Committee:
Professor Benjamin Kerr
Professor Carl T Bergstrom
Biology

Chapter 1. Dispersal and migration are spatially limited in many natural populations. Such limitations can lead to clustering of like types, which weakens competition between unlike types; thus, the rate by which a fitter type displaces an inferior competitor can be affected by the spatial scale of movement. We use a birth-death model to show that, by creating competitive refugia, limited migration can increase the frequency of deleterious mutants at mutation-selection balance.

Chapter 2. For a novel genotype to establish in a population, it must (1) be created, and (2) not be subsequently lost. Recombination is a double-edged sword in this process, potentially fostering creation, but also hastening loss as the novel genotype is being recombined with other genotypes, especially when rare. In this chapter, we find that spatial structure may allow a population to harness the creative side of sex while avoiding its destructive side; that is, it may allow a population to create rare genotypes via recombination, and allow those rare genotypes to persist despite recombination.

Chapter 3. In this chapter, we show that classical rules for predicting competitive outcomes in continuous-time systems are appropriate for a certain subset of discrete-time systems, which motivates a new discrete-time competitive exclusion principle. However, in discrete-time systems in which our proof's assumptions are not held, we show that classical rules can fail dramatically.

Chapter 1

Tipping the mutation-selection balance: Limited migration increases the frequency of deleterious mutants

Jacob D Cooper[*,†], Claudia Neuhauser[‡], Antony M Dean[§], Benjamin Kerr[*,†]

[*] *Department of Biology, University of Washington, Seattle, WA*
[†] *BEACON Center for the Study of Evolution in Action, University of Washington, Seattle, WA*
[‡] *Biomedical Informatics and Computational Biology, University of Minnesota, Rochester, MN*
[§] *College of Ecology and Evolution, Sun Yat-sen University, Guangzhau, China*

Running title:

Tipping the Mutation-Selection Balance

Corresponding author:

Jacob D Cooper
University of Washington
Department of Biology
Box 351800
Seattle, WA 98195-1800

phone: (206) 221-7026

email: yankel@uw.edu

Keywords:

population genetics

fitness landscape

adaptive valley crossing

spatial structure

moment closure

Abstract: Typical mutation-selection models assume well-mixed populations, but dispersal and migration within many natural populations is spatially limited. Such limitations can lead to enhanced variation among locations as different types become clustered in different places. Such clustering weakens competition between unlike types relative to competition between like types; thus, the rate by which a fitter type displaces an inferior competitor can be affected by the spatial scale of movement. In this paper, we use a birth-death model to show that limited migration can affect asexual populations by creating competitive refugia. We use a moment closure approach to show that as population structure is introduced by limiting migration, the equilibrial frequency of deleterious mutants increases. We support and extend the model through stochastic simulation, and we use a spatially explicit cellular automaton approach to corroborate the results. We discuss the implications of these results for standing variation in structured populations and adaptive valley crossing in Wright's "shifting balance" process.

Most mutations affecting fitness appear to be deleterious (see review by Eyre-Walker and Keightley, 2007). A deleterious mutation is expected to persist in a population at a level influenced by the rate at which it is generated and the strength of selection against it. This mutation-selection balance was first developed mathematically by Haldane and Fisher in the 1920's in models that assumed well-mixed populations (Fisher, 1930; Haldane, 1927). However, many natural populations are not well mixed: individuals may not disperse, and even if they do, dispersal or migration is often restricted to nearby locations (Evans et al., 2009; Howells et al., 2013; Martin and Canham, 2010). Such limited movement may influence the proportion of deleterious mutants at equilibrium in several ways. In mating diploid populations, the Wahlund effect (in which population-level heterozygosity is depressed when subpopulations differ in allele frequency) combines with dominance relationships among genotypes to influence the frequency of deleterious mutant alleles (Roze and Rousset, 2004; Whitlock, 2002). In haploid asexual models, limiting migration increases between-deme variation and decreases within-deme variation, but the extent to which this shift in variation affects evolution is unclear.

Limitations to migration are not predicted to affect the equilibrium frequency of deleterious mutants in asexual populations when fitness is independent of local composition and density. For instance, Whitlock (2002) finds no effect of migration under a "hard selection" scheme (in which absolute fitness is determined solely by genotype, and thus demes of different compositions may differ in productivity). However, in "soft selection" regimes (in which relative fitness within a deme depends on genotype, but each deme's productivity is the same regardless of composition), demes enriched for mutants are as productive as demes enriched for wild types. Such mutant-rich demes may serve as competitive refugia. Thus, in soft selection schemes, limiting migration can increase the frequencies of deleterious mutants (Roze and Rousset, 2004; Whitlock, 2002).

As mutation, selection and migration occur in a subdivided population, both first-order moments (i.e., the mean) and higher-order moments (i.e., variance, skew, kurtosis, etc.) of allele frequencies across demes can change. Previous models have estimated higher-order moments (or related quantities like F_{ST}) in terms of first-order moments under an assumption of weak selection. In this paper, we take a different approach. We build an ecological model of a subdivided population, in which higher-order moments are dynamic variables. No assumptions about the strength of selection or mutation are required. Using this model, we find that limited migration increases the fraction of mutants at mutation-selection balance. However, our moment-closure approach (in which we express third-order moments in terms of lower-order moments) is exact only under total migration. Thus, our analytical results are accurate when there is minimal subdivision. Similar moment closure approaches have been used to model ecological neutrality, competition, and stability (Bolker and Pacala, 1997; Haegeman and Loreau, 2011; Neuhauser, 2002; Vanpeteghem and Haegeman, 2010). We use computer simulations to confirm that the fraction of mutants at equilibrium increases under limited migration (where the mathematical analysis is approximate). The simulations also show spatial segregation of types, suggesting that mutant-rich areas act as competitive refugia.

MUTATION-SELECTION BALANCE IN A SUBDIVIDED POPULATION

In our model, a population inhabits a metapopulation of patches. Space is implicit in this model; all patches are equally "far" from any given patch. Migration between patches occurs at birth with a specified probability. When the probability is one, every offspring migrates to a random patch, and the population is essentially well mixed. When the probability is lowered slightly from one, there is a small chance an offspring will stay in its natal patch, and thus a modicum of spatial structure is introduced.

Terminology and Life Cycle: Consider two genotypes W and M, for wild type and mutant, respectively, inhabiting a metapopulation with an infinite number of patches. The population size of each patch is finite. In all that follows, genotype indices i and j will be used where $i, j \in \{W, M\}$ and $i \neq j$. The per capita birth rate of genotype i is given by $F_i(n_i, n_j) = f_i - \beta_i(n_i + \alpha_{ij} n_j)$, where n_i and n_j are the numbers of genotype i and j in the patch, f_i is the intrinsic growth rate of genotype i, β_i measures the effect of intra-genotypic competition, and α_{ij} is an inter-genotypic conversion factor (i.e., one individual of genotype j counts as α_{ij} individuals of genotype i). Genotype i dies with rate δ_i. Mutation from genotype i to j occurs during the birth process with probability $\mu_{i\to j}$. Migration also occurs at birth, when genotype i migrates to a random patch with probability m_i. The population evolves stochastically in continuous time.

Moment Dynamics: Let $N_i(t)$ be the expected number of genotype i per patch at time t. For typographical convenience, we drop the explicit reference to time dependence in our notation for the terms and equations that follow (e.g., $N_i(t)$ is written N_i). In Appendix 1 we show that

$$\frac{dN_i}{dt} = \left(1 - \mu_{i\to j}\right) N_i \, F_i\left(N_{i|i}, N_{j|i}\right) + \mu_{j\to i} \, N_j \, F_j\left(N_{j|j}, N_{i|j}\right) - \delta_i \, N_i, \qquad (1)$$

where $N_{i|j}$ is the expected number of individuals of genotype i in the patch of a randomly chosen individual of genotype j, with $i, j \in \{W, M\}$.

It can be shown that $N_{i|i} = N_i + \sigma_i^2 / N_i$, where σ_i^2 is the variance in the number of genotype i. When individuals of the given genotype are uniformly distributed (i.e., variance is zero), this reduces to the mean N_i. Similarly, $N_{i|j} = N_i + C/N_j$, where C is the covariance between the numbers of genotypes i and j. When the two genotypes are independently distributed (i.e., covariance is zero) this

term reduces to the mean N_i. Covariance may be positive, indicating association between types, or negative, indicating segregation of types.

Thus the dynamics of the first order moments N_i and N_j rely on second order moments σ_i^2, σ_j^2, and C. The equations governing the dynamics of these second order moments involve third order moments, the differential equations for the third order moments involve fourth order moments, and so on. Our task is similar to Hercules' battle with the Hydra (in spirit, not magnitude!). With each Hydra head Hercules sliced off, new heads popped up in its place. For each moment dynamical equation we describe, the description of new, higher-order moment equations becomes necessary. We must find a way to stem the endless flow of higher-order moments. Hercules seared the necks of the Hydra to prevent the regrowth of the heads; we close our system of differential equations by a second-order moment closure technique. We approximate third-order moments in terms of lower-order moments (see Appendix 1 for details), thus sealing the endless flow. Our moment closure approximation is exact when migration is absolute (i.e., $m_W = m_M = 1$), and we are not limited by assumptions of near neutrality (Neuhauser, 2002). With this approximation, the dynamics for the second order moments are given by:

$$\frac{d\sigma_i^2}{dt} = \frac{dN_i}{dt} + 2\delta_i(N_i - \sigma_i^2) + 2(1-m_i)\left(1-\mu_{i\to j}\right)\left\{f_i\sigma_i^2 - \beta_i(N_i + 2N_i\sigma_i^2) - \beta_i\alpha_{ij}\left(N_iC + N_j\sigma_i^2\right)\right\}$$
$$+2\left(1-m_j\right)\mu_{j\to i}\left\{f_jC - \beta_j 2N_jC - \beta_j\alpha_{ji}\left(N_iC + N_j\sigma_i^2\right)\right\} \quad (2)$$

$$\frac{dC}{dt} = -\left(\delta_i + \delta_j\right)C + (1-m_i)\left(1-\mu_{i\to j}\right)\left\{f_iC - \beta_i 2N_iC - \beta_i\alpha_{ij}\left(N_jC + N_i\sigma_j^2\right)\right\}$$
$$+\left(1-m_j\right)\mu_{j\to i}\left\{f_j\sigma_j^2 - \beta_j\left(N_j + 2N_j\sigma_j^2\right) - \beta_j\alpha_{ji}\left(N_jC + N_i\sigma_j^2\right)\right\}$$
$$+\left(1-m_j\right)\left(1-\mu_{j\to i}\right)\left\{f_jC - \beta_j 2N_jC - \beta_j\alpha_{ji}\left(N_iC + N_j\sigma_i^2\right)\right\}$$
$$+(1-m_i)\mu_{i\to j}\left\{f_i\sigma_i^2 - \beta_i(N_i + 2N_i\sigma_i^2) - \beta_i\alpha_{ij}\left(N_iC + N_j\sigma_i^2\right)\right\} \quad (3)$$

Mutation-Selection Balance: Our dynamical system contains many parameters. To simplify matters, we assume $m_W = m_M = m$, $f_W = f_M = f$, $\beta_W = \beta_M = \beta$, $\alpha_{WM} = \alpha_{MW} = 1$, $\mu_{W\to M} = \mu$, and $\mu_{M\to W} = 0$. Thus, we assume our genotypes are identical in all parameters except their death rates, which define a W to M mutation as deleterious (i.e. $\delta_M > \delta_W > 0$), and their mutation rates. Consequently, we only consider viability selection in this analysis, though we simulate other possibilities below. We have also assumed that intra-genotypic competition is identical to inter-genotypic competition (the α parameters are set to unity), and that back mutation does not occur. This might be realistic if the mutation from wild type to the mutant involves a deletion, but even if this mutation is a base substitution, the density of mutants is often so low that back mutation does not greatly affect our results (see simulations below).

In Appendix 2, we derive the mutant fraction of the population at equilibrium under full migration ($m = 1$). Because the fraction of mutants cannot be greater than one, there are parameter constraints on the analysis to ensure mutation does not "overwhelm" selection. Within those parameter constraints, the fraction of mutants at mutation-selection balance is

$$\Phi = \frac{\mu\delta_W}{(1-\mu)(\delta_M-\delta_W)}. \quad (4)$$

Like the classical result for a panmictic haploid population, for which $\Phi = \frac{\mu}{s}$ where $1 - s$ is the fitness of a mutant relative to a wild-type (Crow and Kimura, 1970), our expression is proportional to μ (for small μ) and inversely proportional to a measure of the selective disadvantage of the mutant ($\frac{\delta_M}{\delta_W} - 1$).

How does this fraction change as spatial structure is introduced; that is, what happens to Φ as m is lowered from unity? Since Equations (2) and (3) are exact for $m = 1$, the partial derivative of Φ with respect to m can be computed exactly at $m = 1$ (Neuhauser, 2002). In Appendix 3, we derive the following:

$$\left.\frac{\partial \Phi}{\partial m}\right|_{m=1} = -\frac{\beta\mu}{(1-\mu)^2\delta_M\{(\delta_M/\delta_W)^2-1\}}. \quad (5)$$

This expression demonstrates that $\left.\frac{\partial \Phi}{\partial m}\right|_{m=1} < 0$ for $0 < \mu < 1$, so the fraction of deleterious mutants at equilibrium always increases when a small amount of structure is introduced into the model.

Simulation of the Spatial Model

Our analysis is exact when all offspring migrate, but becomes approximate as soon as some offspring remain in their natal patches. How well do the approximations capture actual dynamics? Here, we explore the model via simulation.

In the simulation, we seed a finite (but large) number of patches *P* with wild type and mutant individuals, and simulate evolution using a Gillespie algorithm in which birth and death events occur stochastically (see Appendix 4 for details). In simulation runs with absolute migration, all first order moments and second order moments approach our analytic predictions as equilibrium is reached, even when initialized far from the calculated equilibrium (Sup. Fig. 1). This is expected, as our analysis is exact when migration is absolute. As the probability of migration is lowered from unity, our analysis becomes approximate. Figure 1 shows simulation results across a range of migration probabilities, and the analytical prediction extrapolated from Equation (5). At high levels of migration, the simulation corresponds well with the analysis, with Φ following its derivative calculated at $m = 1$ (Fig. 1, inset). As migration drops further, the mutant frequency rises faster than the linear extrapolation from our analytical model (Fig. 1). The correspondence between our finite simulation and our deterministic analysis for high migration indicates that the number of patches *P* is large enough for the metapopulation to behave deterministically. Moreover, results are not appreciably affected when fewer patches are used (Sup. Fig. 2B). Results are also not appreciably affected when back mutation is allowed (Sup. Fig. 2A).

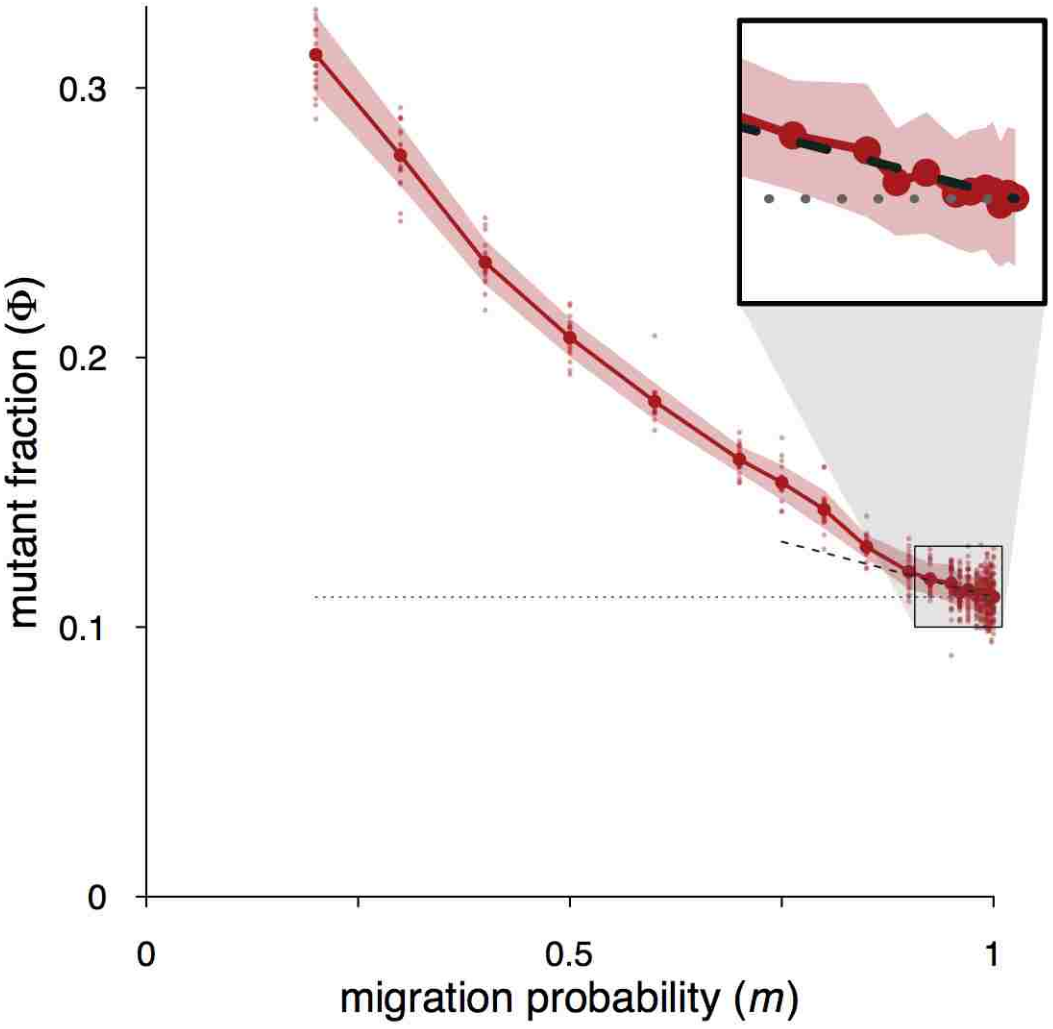

Figure 1. Stochastic simulation under various migration rates. Frequency of deleterious mutants at mutation-selection balance across various probabilities of migration as found by simulation (red circles), compared to the *m*=1 derivative of our analytical model (black dashed line). The analytically calculated mutant fraction at full migration is given as a gray dotted horizontal line for comparison. At high migration probabilities, the simulation results agree well with our analytical model (see inset). As the probability of migration decreases further from unity, the fraction of deleterious mutants increases faster than the analytical extrapolation. Large data points and shading represent mean values and standard deviation of 20-40 replicate simulations (small data points) using parameter values $P = 10^4$, $f = 0.5$, $\beta = 0.2$, $\mu = 0.1$, $\delta_W = 0.05$, $\delta_M = 0.1$, corresponding to a per-patch carrying capacity of approximately $\frac{f-\delta_W}{\beta} = 2.25$.

Parameters for Figure 1 were chosen to illustrate a large effect of limited migration on the mutant fraction at mutation-selection balance. When the competition parameter β is decreased, $\mathrm{abs}\left(\frac{\partial \Phi}{\partial m}\Big|_{m=1}\right)$ is proportionately decreased (see Eq. 5) and the per-patch carrying capacity is increased, but the simulated mutant frequency still rises faster than the linear extrapolation from our model (Sup. Fig. 2C). Similar results to those shown in Figure 1 occur when both the mutation rate and the selective disadvantage of mutants are decreased (Sup. Fig. 2D).

To see why limited migration increases the fraction of deleterious mutants in a population, we follow a simulation (Fig. 2) as it transitions from absolute migration to limited migration (i.e., $m = 1$ to $m = 0.5$). We see that when limited migration is introduced, the mutant frequency increases (Fig. 2A), the variance in mutant density increases (i.e., the mutants become more clumped), and the covariance between the densities of the two genotypes becomes negative (i.e., patches with many wild-type genotypes tend to have fewer mutant genotypes, and *vice versa*) (Fig. 2B).

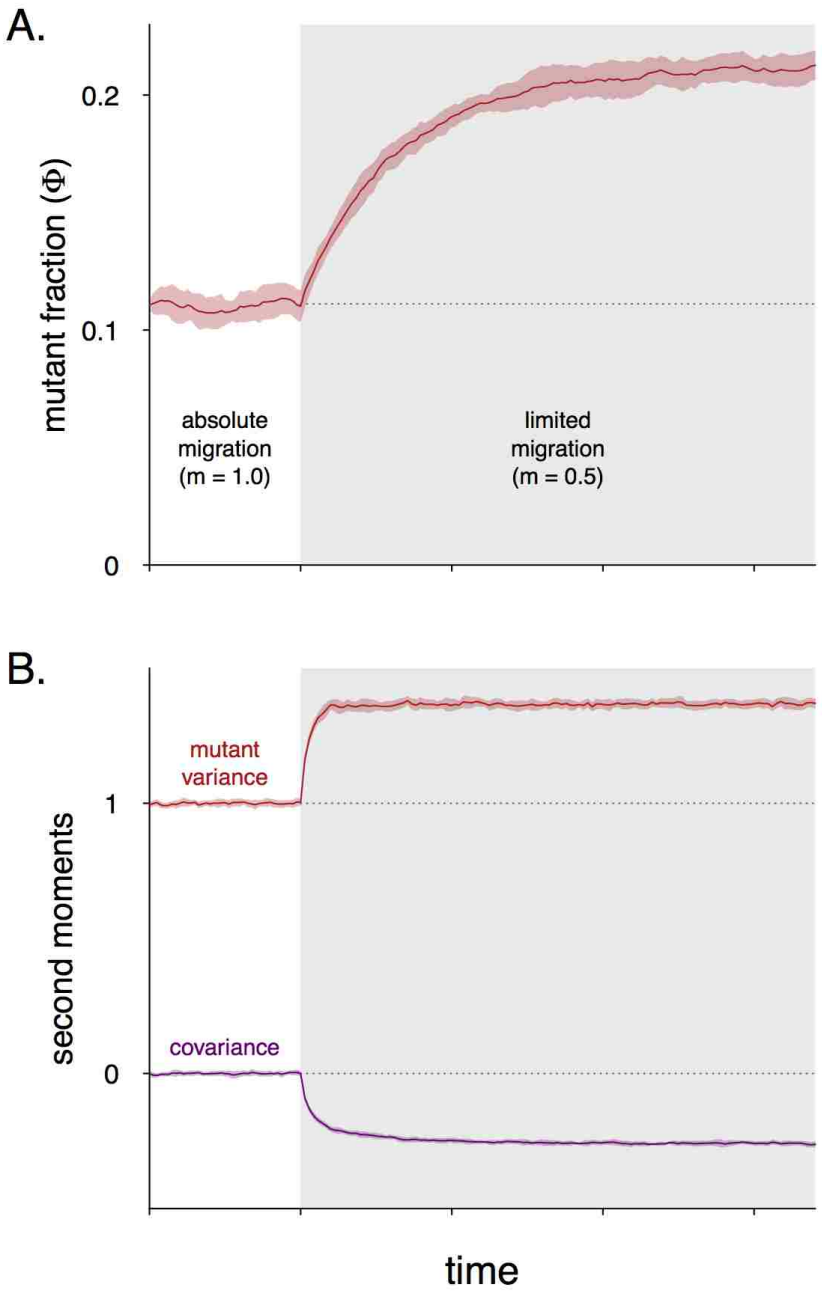

Figure 2. A simulated shift in the probability of migration. When migration becomes limited (grey-shaded portion of plots), the increase in deleterious mutant frequency (A) coincides with an increase in the variance in mutant density and a decrease in the covariance between mutant and wild type densities (B, variances are divided by the means of their corresponding variables, and covariance is divided by the product of the roots of the two means). Time units are relative, and defined by a Gillespie algorithm described in Appendix 4. Solid lines and colored shading represent the mean ± SD of 16 replicate simulations using the parameter values listed in Figure 1.

Such spatial segregation leads to an increase in the fraction of inhabited patches that house mutant-only populations (Sup. Fig. 3A). The fraction of mutants in mutant-only patches also increases as the migration rate decreases (Sup. Fig. 3B). Notably, the fraction of mutants in patches that also house wild type genotypes does not increase as the migration rate decreases (Sup. Fig. 3B). Thus, the increase of mutants in mutant-only patches may suffice to explain the overall increase in mutants at limited migration rates.

We conclude that limited migration leads to a higher mutant frequency at mutation-selection balance because the less fit mutant is able to escape competition with the wild type due to spatial segregation. Thus, mutant-rich patches are competitive refugia that allow the mutant genotype to persist in relative isolation from the competitively superior wild type. If this explanation is correct, limited migration should safeguard deleterious mutants regardless of whether selection occurs via differences in viability or fecundity, whether space is explicit or implicit, and whether the spatially distributed units are populations or individuals.

A LATTICE-BASED APPROACH

Our next approach considers individuals that are embedded in a lattice. Here, unlike our first approach, (a) space is explicit, (b) population structure varies with dispersal distance, (c) the "patches" house individuals rather than subpopulations, and (d) we consider both viability and fecundity selection. A similar lattice-based approach has been used to explore many eco-evolutionary aspects of spatially structured populations, including the invasion of rare types, species coexistence, host-parasite evolution, spatial structuring of communities, and evolutionary trajectories (Débarre et al., 2012; Durrett and Levin, 1997; Hauert and Doebeli, 2004; Kerr et al., 2002).

In our simulation, we consider two haploid asexual genotypes: wild type (W) and mutant (M). These genotypes occupy an $L \times L$ regular square lattice with periodic boundaries (i.e., a toroidal geometry). Each lattice point may take one of three states: empty, wild type, or mutant. At each update, a point is chosen at random. If this focal point is "filled" with a wild type, the wild type dies with probability δ_W^*, giving a transformation to the empty state. Likewise, a mutant that is chosen will die with probability δ_M^* (where $\delta_M^* \geq \delta_W^* > 0$).

If the focal point is already empty, then a birth event can occur, where an individual in a pre-defined neighborhood of the focal point produces an offspring that fills the focal point (giving a transformation to a filled state). Let x_W and x_M be the fraction of the focal point's neighborhood occupied by wild type and mutant lattice points, respectively. Then with probabilities $f_W^* x_W$ and $f_M^* x_M$ the parent of the individual "born into" the focal point is wild type and mutant, respectively. The parameters f_W^* and f_M^* represent the fecundities of wild-type and mutant individuals (where $0 \leq f_M^* \leq f_W^* \leq 1$). The focal point stays empty with probability $1 - f_W^* x_W - f_M^* x_M$. Mutation occurs at birth: from wild type to mutant with probability $\mu_{W \to M}^*$, and from mutant to wild type with probability $\mu_{M \to W}^*$. The degree of population structure is controlled by adjusting the size of the neighborhood around any focal point (effectively altering the distribution of distance at dispersal). We focus on three cases: a von Neumann neighborhood (where the lattice points immediately to the north, east, south and west of the focal point comprise the neighborhood), a Moore neighborhood (where the eight lattice points nearest the focal point constitute the neighborhood), and a Global neighborhood (where the entire lattice, minus the focal point, comprises the neighborhood). Thus, the evolving population can range from highly structured (von Neumann neighborhood) to effectively well mixed (Global neighborhood).

Figure 3 shows that smaller dispersal neighborhoods lead to higher mutant frequencies at equilibrium, corroborating our prior analysis. This pattern holds under both pure viability selection ($\delta_M^* > \delta_W^*$ and $f_M^* = f_W^*$) and pure fecundity selection ($\delta_M^* = \delta_W^*$ and $f_M^* < f_W^*$).

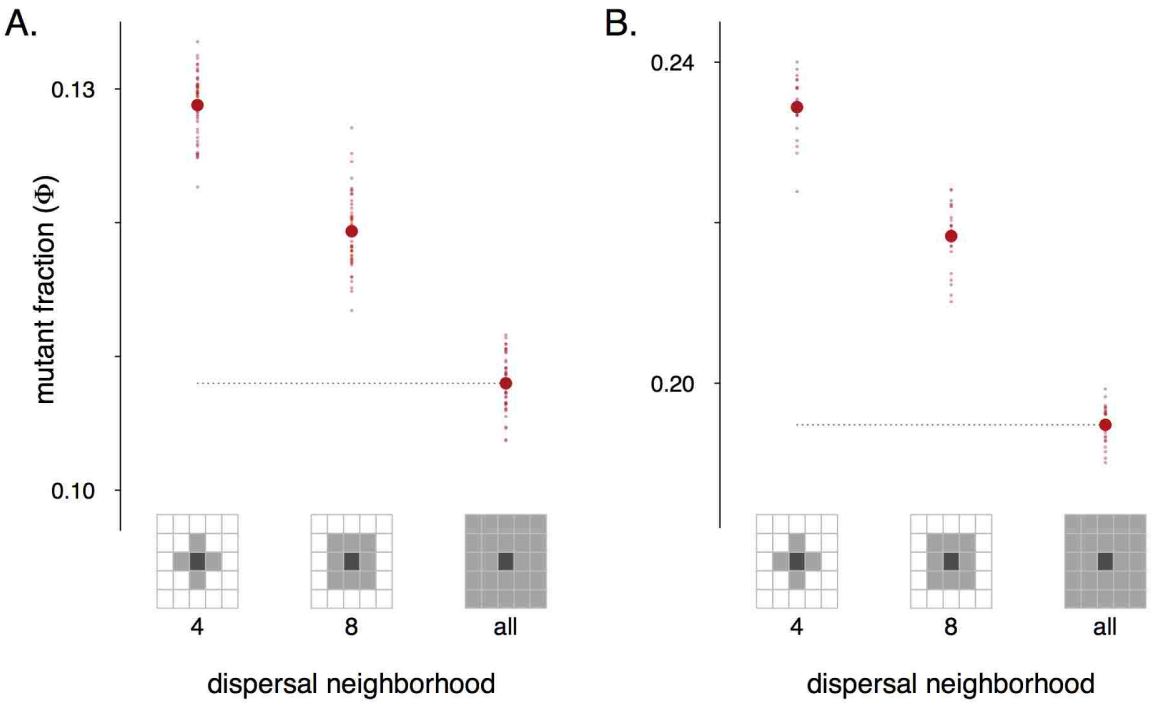

Figure 3. Lattice-based simulation results. The frequency of deleterious mutants at mutation-selection balance across various neighborhood sizes in lattice-based simulations with viability selection (A) or fecundity selection (B). As dispersal is limited to smaller neighborhoods, the frequency of deleterious mutants increases. Large data points represent mean values of 24 replicate simulations (small data points) using parameter values $L = 200$, $\mu_{W\to M}^* = 0.1$, $\mu_{M\to W}^* = 0.02$, and either viability selection (A, with $\delta_W^* = 0.1$, $\delta_M^* = 0.2$, $f_W^* = f_M^* = 1$) or fecundity selection (B, with $\delta_W^* = \delta_M^* = 0.1$, $f_W^* = 1$, $f_M^* = 0.5$).

DISCUSSION

We find analytically and computationally that limited migration increases the frequency of deleterious mutants, and this increase is not restricted to a specific form of space or mode of selection. Prior models of selection in metapopulations have shown effects of limited migration when local interactions are defined by mating, or when mutant-rich demes have similar productivity to wild type enriched demes, and can thus act as competitive refugia for mutants (Glémin et al., 2003; Roze and Rousset, 2004; Whitlock, 2002). In this paper, we embedded competition in an explicitly ecological framework, which allows us to manifest local interactions explicitly as density-dependent fecundity. We used a moment closure approach that expresses higher-order moments in terms of lower-order moments, therefore allowing those higher-order moments to vary dynamically as we began to limit migration. We showed that limited migration can affect asexual populations by segregating types. Essentially, limiting migration has no effect on the generation of mutants, but hampers the effective strength of selection (Cherry and Wakeley, 2003) by sheltering alleles from global competition, and so tips the mutation-selection balance in favor of deleterious mutations. Generally, whenever there is both variation in localities and local interaction, migration rate will be a salient factor in determining the frequency of deleterious mutants.

Mutant frequency is sometimes used to estimate mutation rates of microbes. Using such a method, a structured environment may appear mutagenic because a higher frequency of mutants is found. For example, Bjedov *et al.* (2003) find a disparity in mutant frequencies between liquid and agar bacterial cultures, and attribute it to oxidative stress incurred during colonial growth on agar. This explanation is certainly plausible, but the colony structure itself may contribute to the increased mutant frequency. When going from an unstructured to a structured environment (e.g., a flask to an agar plate), the frequency of deleterious mutants may increase even if the mutation rate is constant.

Adaptive valley crossing: If a single deleterious mutation is complemented by a second mutation that improves the fitness of the organism above the wild type, the frequency (and number) of the original mutant may be relevant for crossing "adaptive valleys". Recent theoretical studies have elucidated how well-mixed populations cross adaptive valleys, and at what rate (Weissman et al., 2010, 2009). However, Sewall Wright's shifting balance process is predicated on the idea that, collectively, semi-isolated subpopulations would explore a landscape in a way unavailable to well-mixed populations (Pigliucci, 2008; Wright, 1988, 1932). To cross a valley, a population must first discover a new peak, and then have the peak genotype spread through the population. Increasing migration between separated patches hinders exploration of novel genotypes (Whitlock, 2003), but, once a beneficial genotype is discovered, the increased migration facilitates its spread (Jain et al., 2011; Rozen et al., 2008). In the rugged landscapes that were the focus of Wright's shifting balance, the rate-limiting step in adaptation may be the discovery of novel genotypes (i.e., finding new peaks) rather than their spread through a population. If this is the case, limited migration may speed the rate of adaptation.

If valley crossing requires multiple "downward" steps, the facilitating effect of limited migration is amplified. Limited migration protects not only deleterious single mutants from competition with wild types, but also relatively deleterious double mutants from competition with single mutants (and wild types). When deleterious double mutants are added to our metapopulation simulation, we see the amplified effect of limited migration on the double-mutant frequency (Fig. 4A); when we add triple mutants, the effect of limited migration amplifies further (Fig. 4B). This effect on double and triple mutants is also observed in our lattice-based approach (Sup. Fig. 4).

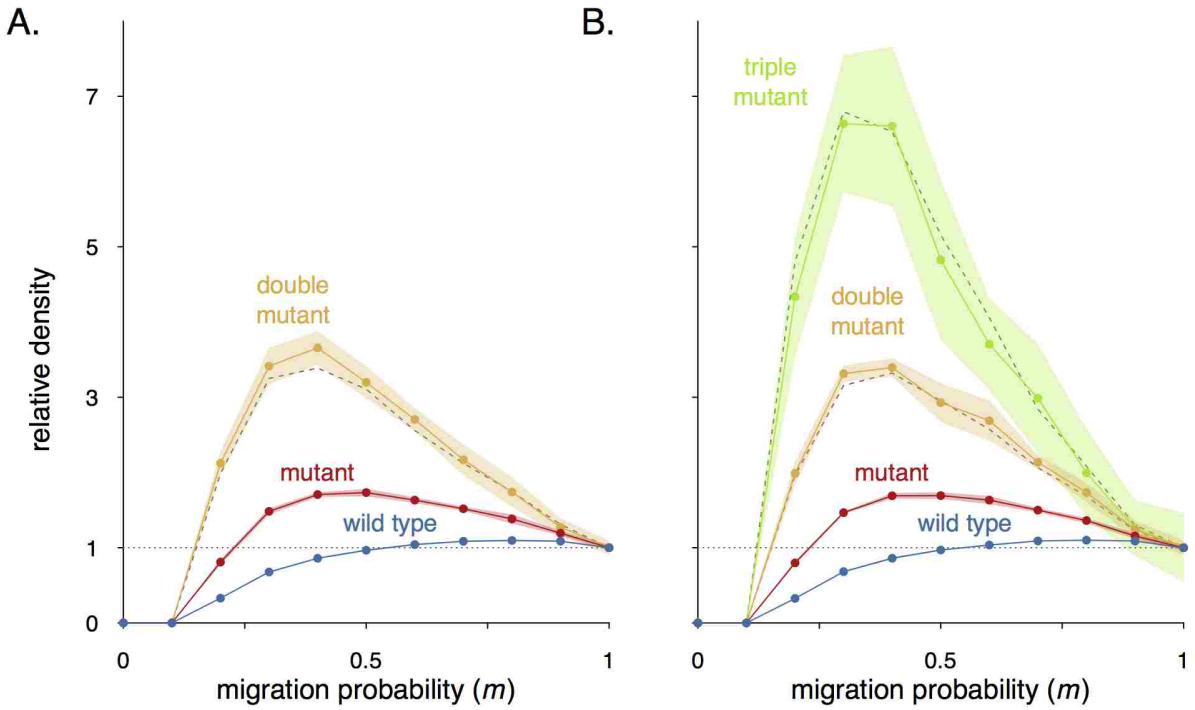

Figure 4. Stochastic simulations with a chain of sequential deleterious mutants in a metapopulation approach. The wild-type genotype yields the first mutant via mutation; the first mutant yields the relatively deleterious double mutant via mutation; and so on. The density of each genotype is shown relative to its density in a well-mixed population (given by the dotted line at unity). The effect of migration probability on relative density in a community with two (A) and three (B) mutants are shown. Points and colored shading represent the mean ± SD of 12 replicate simulations, while dashed lines roughly matching the double-mutant frequency represent the square of the mutant to wild-type ratio, multiplied by the wild-type density, for each *m*. In (B), the cubes of the ratios are also shown, roughly matching the triple-mutant density. Parameter values used in this simulation are: $P = 10^4$, $f = 0.5$, $\beta = 0.2$, $\mu_{W\to M} = \mu_{M\to M2} = \mu_{M2\to M3} = 0.1$, $\mu_{M3\to M2} = \mu_{M2\to M} = \mu_{M\to W} = 0.01$, $\delta_W = 0.05$, $\delta_M = 0.1$, $\delta_{M2} = 0.2$, $\delta_{M3} = 0.4$.

For sufficiently wide valleys, a population starting with only wild type individuals may discover the peak genotype faster when its migration is limited (Fig. 5). For certain parameter values, a population whose migration is limited may cross even the narrowest valley—one deleterious mutant between two peak genotypes—faster than an unstructured population (Bitbol and Schwab, 2014). Note

that when only upward steps are required for adaptation (e.g., a smooth landscape) then the rate-limiting step in adaptation is the spread of beneficial genotypes, and thus limited migration will inhibit adaptation (Kryazhimskiy et al., 2012).

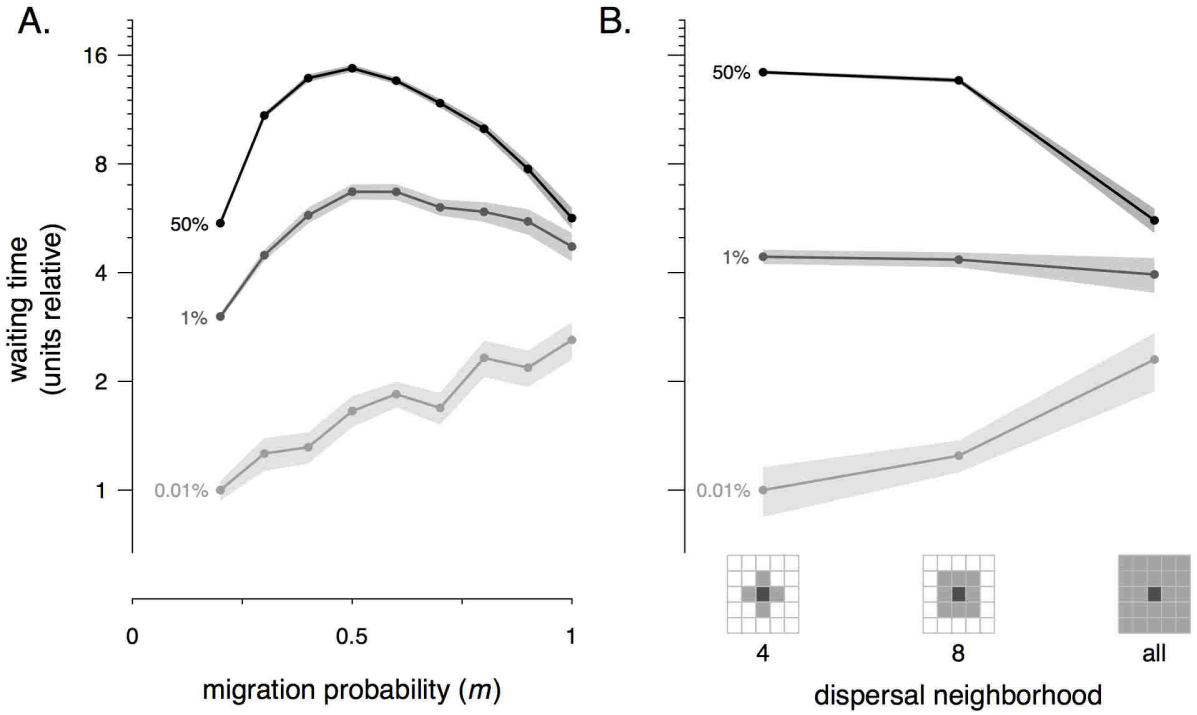

Figure 5. Discovery versus spread in simulated populations. Both metapopulation (A) and lattice (B) simulations were initialized with wild type genotypes only. There are three successively more deleterious mutants comprising a valley between the wild type genotype and a highly beneficial mutant (accessible from the third deleterious mutant). The waiting time before the beneficial mutant reaches a given frequency is shown. As migration becomes more limited, the waiting time to the discovery of the beneficial mutant decreases (as m decreases from 1, the 0.01% profile drops; as the dispersal neighborhood shrinks, the 0.01% profile drops). However, a greater degree of structure inhibits the spread of these beneficial mutants (and thus the time to reach a substantial frequency of the beneficial mutant can increase under initial limitations to migration—see 1% and 50% trajectories). Extremely limited migration decreases total population size, facilitating spread. Fixation does not occur as back mutation is allowed and the numbers of patches are large. Points and shaded regions represent the mean ± SEM of 24-36 (A) or 16 (B) replicate simulations using parameter values $f = 0.5$, $\beta = 0.2$, $\mu_{W\to M} = \mu_{M\to M2} = \mu_{M2\to M3} = 0.1$, $\mu_{M3\to M2} = \mu_{M2\to M} = \mu_{M\to W} = 0.01$, $\delta_W = 0.05$, $\delta_M = 0.1$, $\delta_{M2} = 0.2$, $\delta_{M3} = 0.4$, $\delta_{M4} = 0.025$. For (A), $P = 10^4$. For (B) $L = 200$.

The limited migration of individuals generally slows the spread of advantageous traits. However, it is precisely this dampening of competition that can allow spatially structured populations to safeguard deleterious mutants. By harboring this diversity, it may be possible for structured populations to discover novel genotypes faster, even if the benefit spreads more slowly.

LITERATURE CITED

Bitbol, A.-F., Schwab, D.J., 2014. Quantifying the Role of Population Subdivision in Evolution on Rugged Fitness Landscapes. PLoS Comput Biol 10, e1003778. doi:10.1371/journal.pcbi.1003778

Bjedov, I., Tenaillon, O., Gérard, B., Souza, V., Denamur, E., Radman, M., Taddei, F., Matic, I., 2003. Stress-induced mutagenesis in bacteria. Science 300, 1404–1409. doi:10.1126/science.1082240

Bolker, B., Pacala, S.W., 1997. Using moment equations to understand stochastically driven spatial pattern formation in ecological systems. Theoretical population biology 52, 179–197.

Cherry, J.L., Wakeley, J., 2003. A Diffusion Approximation for Selection and Drift in a Subdivided Population. Genetics 163, 421–428.

Crow, J.F., Kimura, M., 1970. An introduction to population genetics theory.

Débarre, F., Lion, S., Baalen, Gandon, S., 2012. Evolution of Host Life-History Traits in a Spatially Structured Host-Parasite System. The American Naturalist 179, 52–63. doi:10.1086/663199

Durrett, R., Levin, S., 1997. Allelopathy in spatially distributed populations. Journal of Theoretical Biology 185, 165–171.

Evans, K.M., Chepurnov, V.A., Sluiman, H.J., Thomas, S.J., Spears, B.M., Mann, D.G., 2009. Highly Differentiated Populations of the Freshwater Diatom Sellaphora capitata Suggest Limited Dispersal and Opportunities for Allopatric Speciation. Protist 160, 386–396. doi:10.1016/j.protis.2009.02.001

Eyre-Walker, A., Keightley, P.D., 2007. The distribution of fitness effects of new mutations. Nat. Rev. Genet. 8, 610–618. doi:10.1038/nrg2146

Fisher, R.A., 1930. The Distribution of Gene Ratios for Rare Mutations. Proc. Roy. Soc. Edinburgh 50, 205–220.

Gillespie, D.T., 1977. Exact stochastic simulation of coupled chemical reactions. J. Phys. Chem. 81, 2340–2361. doi:10.1021/j100540a008

Glémin, S., Ronfort, J., Bataillon, T., 2003. Patterns of inbreeding depression and architecture of the load in subdivided populations. Genetics 165, 2193–2212.

Haegeman, B., Loreau, M., 2011. A mathematical synthesis of niche and neutral theories in community ecology. Journal of Theoretical Biology 269, 150–165.

Haldane, J.B.S., 1927. A Mathematical Theory of Natural and Artificial Selection, Part V: Selection and Mutation. Mathematical Proceedings of the Cambridge Philosophical Society 23, 838–844. doi:10.1017/S0305004100015644

Hauert, C., Doebeli, M., 2004. Spatial structure often inhibits the evolution of cooperation in the snowdrift game. Nature 428, 643–646.

Howells, E.J., Willis, B.L., Bay, L.K., van Oppen, M.J.H., 2013. Spatial and temporal genetic structure of Symbiodinium populations within a common reef-building coral on the Great Barrier Reef. Molecular Ecology 22, 3693–3708. doi:10.1111/mec.12342

Jain, K., Krug, J., Park, S.-C., 2011. Evolutionary Advantage of Small Populations on Complex Fitness Landscapes. Evolution 65, 1945–1955. doi:10.1111/j.1558-5646.2011.01280.x

Kerr, B., Riley, M.A., Feldman, M.W., Bohannan, B.J.M., 2002. Local dispersal promotes biodiversity in a real-life game of rock-paper-scissors. Nature 418, 171–174.

Kryazhimskiy, S., Rice, D.P., Desai, M.M., 2012. Population Subdivision and Adaptation in Asexual Populations of Saccharomyces Cerevisiae. Evolution 66, 1931–1941. doi:10.1111/j.1558-5646.2012.01569.x

Martin, P.H., Canham, C.D., 2010. Dispersal and recruitment limitation in native versus exotic tree species: life-history strategies and Janzen-Connell effects. Oikos 119, 807–824. doi:10.1111/j.1600-0706.2009.17941.x

Neuhauser, C., 2002. Effects of local interactions and local migration on stability. Theoretical population biology 62, 297–308.

Pacala, S.W., Levin, S.A., 1997. Biologically generated spatial pattern and the coexistence of competing species. Spatial ecology. Princeton University Press, Princeton, New Jersey, USA 204–232.

Pigliucci, M., 2008. Sewall Wright's adaptive landscapes: 1932 vs. 1988. Biology and Philosophy 23, 591–603.

Roze, D., Rousset, F., 2004. Joint effects of self-fertilization and population structure on mutation load, inbreeding depression and heterosis. Genetics 167, 1001–1015. doi:10.1534/genetics.103.025148

Rozen, D.E., Habets, M.G.J.L., Handel, A., de Visser, J.A.G.M., 2008. Heterogeneous Adaptive Trajectories of Small Populations on Complex Fitness Landscapes. PLoS ONE 3, e1715. doi:10.1371/journal.pone.0001715

Vanpeteghem, D., Haegeman, B., 2010. An analytical approach to spatio-temporal dynamics of neutral community models. Journal of Mathematical Biology 61, 323–357.

Weissman, D.B., Desai, M.M., Fisher, D.S., Feldman, M.W., 2009. The rate at which asexual populations cross fitness valleys. Theoretical population biology 75, 286–300.

Weissman, D.B., Feldman, M.W., Fisher, D.S., 2010. The rate of fitness-valley crossing in sexual populations. Genetics 186, 1389–1410.

Whitlock, M.C., 2002. Selection, load and inbreeding depression in a large metapopulation. Genetics 160, 1191–1202.

Whitlock, M.C., 2003. Fixation Probability and Time in Subdivided Populations. Genetics 164, 767–779.

Wright, S., 1932. The roles of mutation, inbreeding, crossbreeding and selection in evolution, in: Proceedings of the Sixth International Congress on Genetics. pp. 356–366.

Wright, S., 1988. Surfaces of selective value revisited. The American Naturalist 131, 115–123.

Supplemental Figures

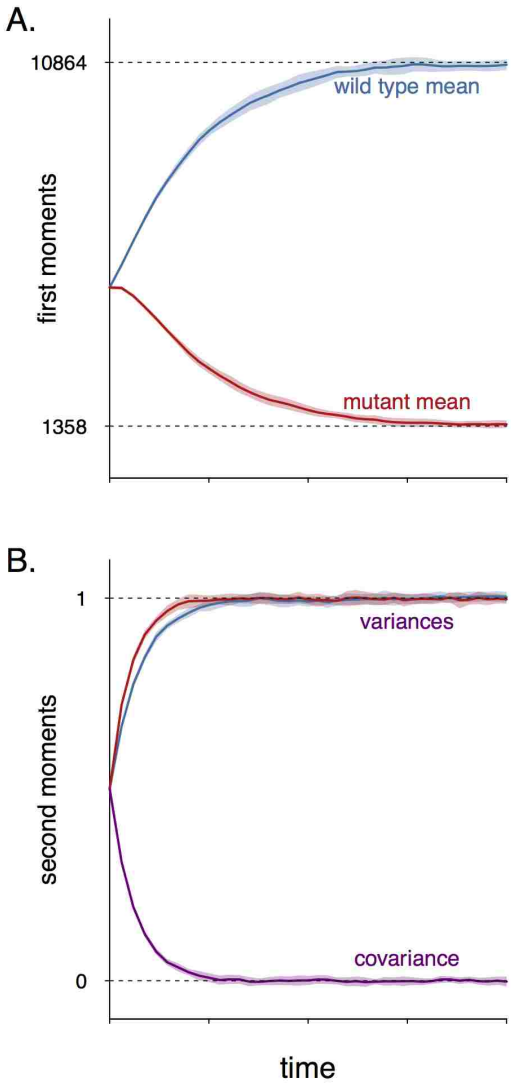

Supplemental Figure 1. Stochastic simulation under full migration ($m = 1$). The equilibrium values for all first and second order moments (dashed lines) are calculated from the model. The initial conditions used for the simulation are far removed from these equilibria: each patch starts either empty or with one wild type and one mutant, each with equal probability. All first order moments (A) and second order moments (B) converged to their expected values. In (B), variances are divided by the means of their corresponding variables, and covariance is divided by the product of the roots of the two means. Time units are relative, and defined by a Gillespie algorithm described in Appendix 4. Solid lines and shaded areas represent means ± SDs of eight replicate simulations using parameter values $P = 10^4$, $f = 0.5$, $\beta = 0.2$, $\mu = 0.1$, $\delta_W = 0.05$, $\delta_M = 0.1$.

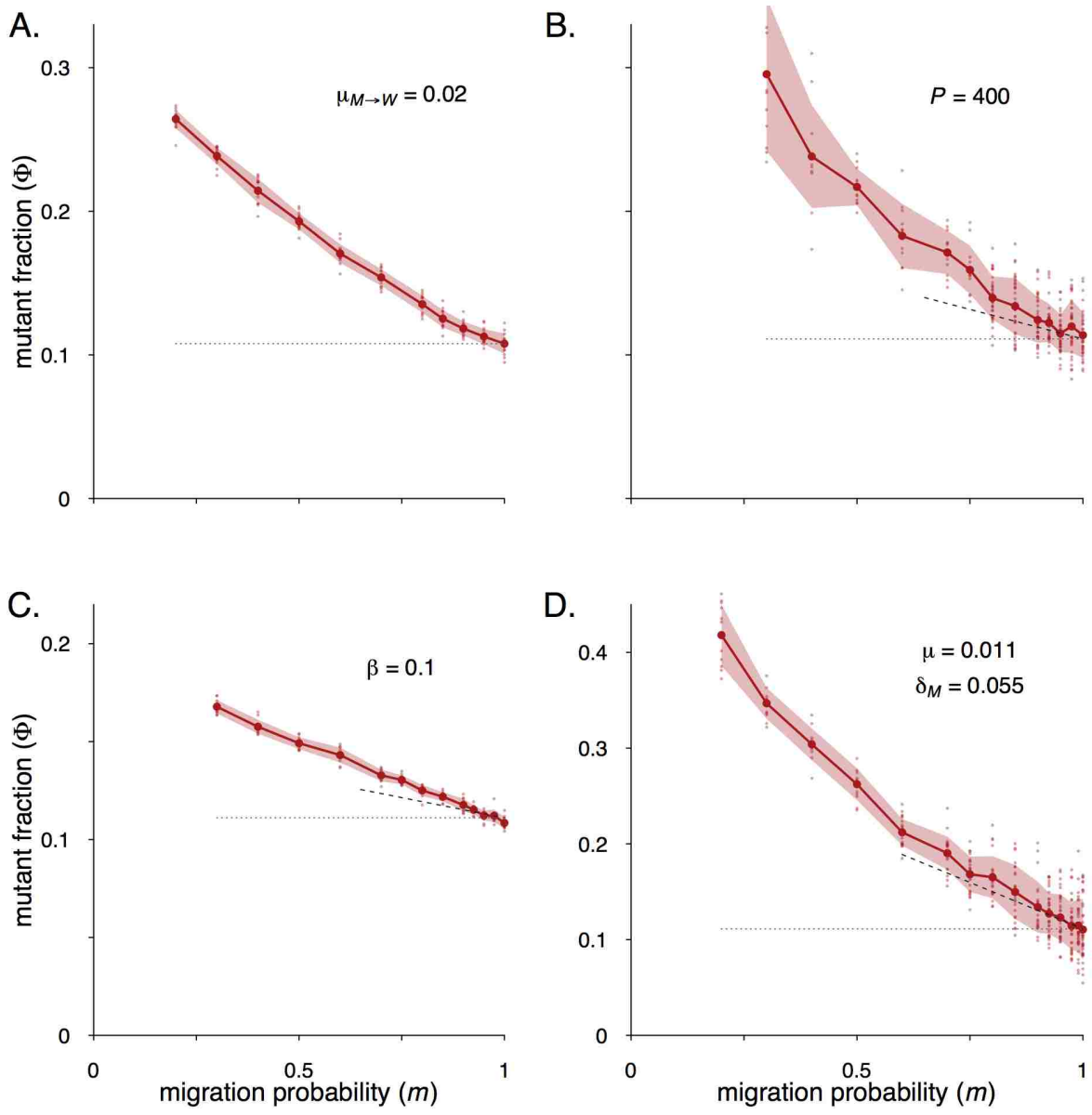

Supplemental Figure 2. Stochastic simulations under various migration rates, with parameters identical to those used for Figure 1 ($P = 10^4$, $f = 0.5$, $\beta = 0.2$, $\mu = 0.1$, $\delta_W = 0.05$, $\delta_M = 0.1$) except with (A) non-zero back mutation rate, (B) fewer patches, (C) decreased competition parameter, and (D) decreased selective disadvantage of mutants with a compensating decrease in mutation rate (see Eq. 4). Frequency of deleterious mutants at mutation-selection balance plotted across various probabilities of migration as found by simulation (red circles), compared to the *m*=1 derivative of our analytical model (black dashed line). The simulated (A) or analytically calculated (B, C, D) mutant fraction at full migration is given as a gray dotted horizontal line for comparison. Large data points and shading represent means ± SDs of 12-36 replicate simulations (small data points).

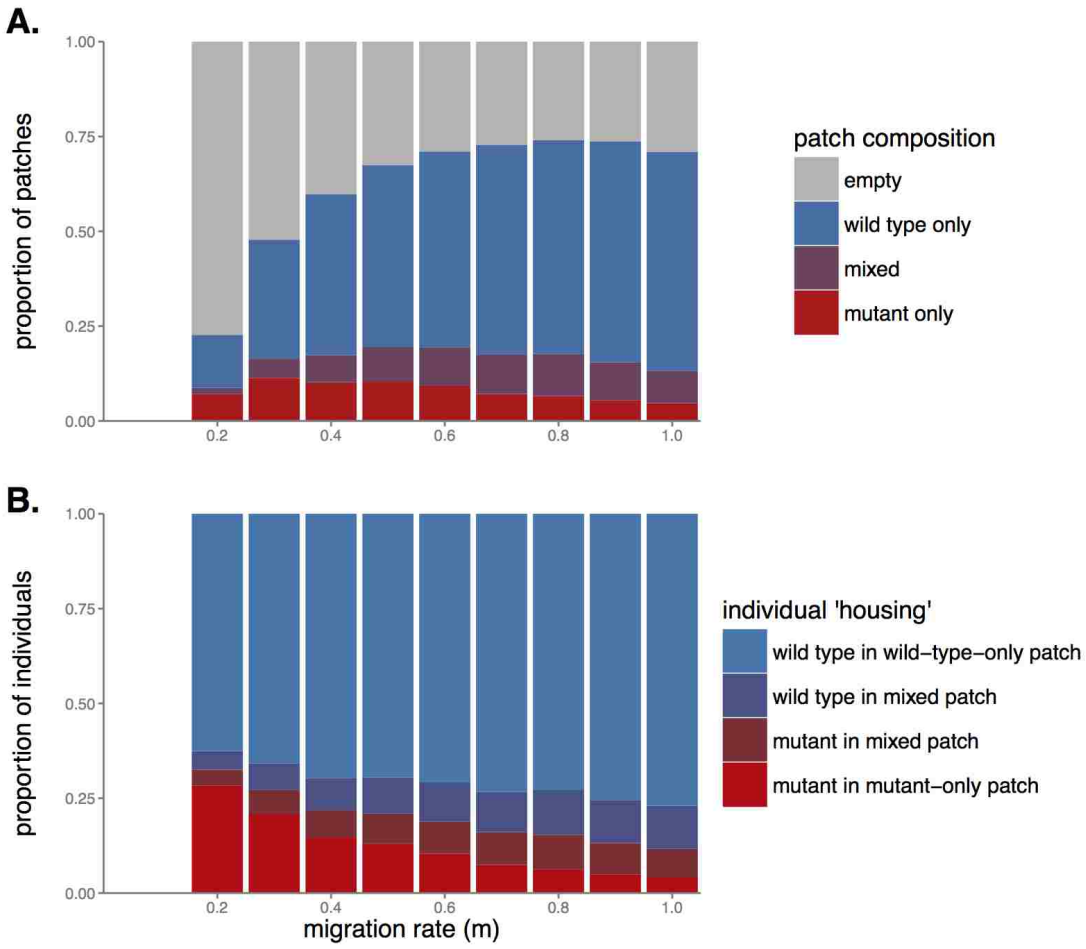

Supplemental Figure 3. Patches as competitive refugia for deleterious mutants. The proportion of homotypic, heterotypic, and empty patches at approximately steady-state for a range of migration rates is shown (A). At very low migration rates, the frequency of empty patches increases due to the low rate of reseeding after stochastic within-patch extinctions. The proportion of wild type and mutant individuals 'housed' in homotypic and heterotypic patches is also shown (B). Each bar represents the mean values of two replicate simulations using parameter values $P = 10^4$, $f = 0.5$, $\beta = 0.2$, $\mu = 0.1$, $\delta_W = 0.05$, $\delta_M = 0.1$.

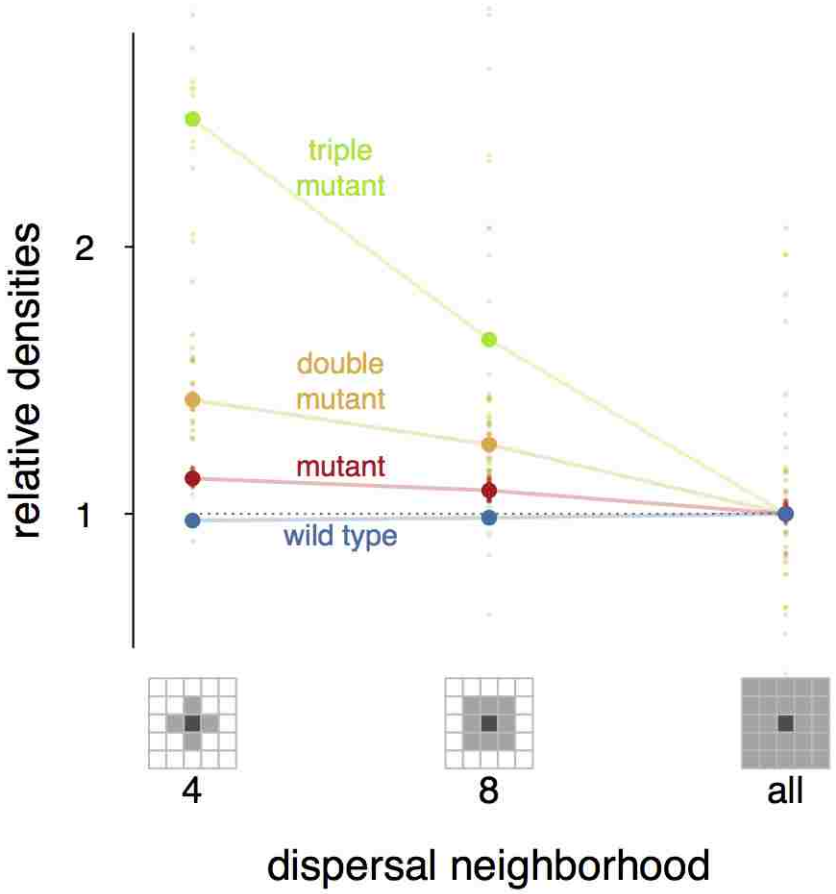

Supplemental Figure 4. Lattice-based simulations with a chain of sequential deleterious mutants (as in Figure 4). The density of each genotype is shown relative to its density in a population with a global neighborhood (given by the value of unity). Large data points represent mean values of 24 replicate simulations (small data points) using parameter values $L = 200$, $\mu^*_{W\to M} = \mu^*_{M\to M2} = \mu^*_{M2\to M3} = 0.1$, $\mu^*_{M3\to M2} = \mu^*_{M2\to M} = \mu^*_{M\to W} = 0.02$, $\delta^*_W = 0.1$, $\delta^*_M = 0.2$, $\delta^*_{M2} = 0.4$, $\delta^*_{M3} = 0.8$, $f^*_W = f^*_M = f^*_{M2} = f^*_{M3} = 1$.

Appendices

Appendix 1: Moment Equations

Mean Density Dynamics

In this appendix, we derive the dynamical equations for our first and second-order moments. We assume our population inhabits a metapopulation of infinite patches (each of which houses a finite population), allowing us to use expectation values for our patch dynamics. We start with the dynamics of the mean genotype abundances. Let $q_i(t)$ be a random variable giving the number of individuals of genotype $i \in \{W, M\}$ within a randomly selected patch at time t. If we consider a period of time, Δt, small enough that the probabilty of more than one event occuring during that interval is vanishing small, we have the following:

$$q_i(t+\Delta t) = \begin{cases} q_i(t) - 1 & \text{with probability } P_i^- \\ q_i(t) + 1 & \text{with probability } P_i^+ \end{cases}, \tag{A1.1}$$

where

$$P_i^- = \delta_i q_i(t) \Delta t, \tag{A1.2}$$

and

$$\begin{aligned} P_i^+ = {} & (1-m_i)(1-\mu_{i\to j}) F_i\left(q_i(t), q_j(t)\right) q_i(t)\Delta t + (1-m_j)\mu_{j\to i} F_j\left(q_j(t), q_i(t)\right) q_j(t)\Delta t \\ & + m_i(1-\mu_{i\to j}) E\left[F_i\left(q_i(t), q_j(t)\right) q_i(t)\right]\Delta t + m_j \mu_{j\to i} E\left[F_j\left(q_j(t), q_i(t)\right) q_j(t)\right]\Delta t. \end{aligned} \tag{A1.3}$$

where E is the expectation value over all patches. Thus, the expected change in q_i over our small interval of time is given by:

$$E[\Delta q_i] = E[P_i^+ - P_i^-]. \tag{A1.4}$$

For typographical convenience, we drop the explicit time dependence in our notation for the terms and equations that follow. We use the following notations

$$N_i = E[q_i],$$

$$\sigma_i^2 = \mathrm{var}[q_i],$$

$$C = \mathrm{cov}[q_i, q_j] = \mathrm{cov}[q_j, q_i],$$

and we have the following relations

$$E[q_i^2] = N_i^2 + \sigma_i^2, \tag{A1.5}$$

$$E[q_i q_j] = N_i N_j + C. \tag{A1.6}$$

Using (A1.5), (A1.6), and our per capita birth rate of $F_i(n_i, n_j) = f_i - \beta_i(n_i + \alpha_{ij} n_j)$ we can rewrite (A1.4) as follows:

$$\frac{E[\Delta q_i]}{\Delta t} = -\delta_i N_i + (1 - \mu_{i\to j})\left\{f_i N_i - \beta_i\left((N_i^2 + \sigma_i^2) + \alpha_{ij}(N_i N_j + C)\right)\right\}$$
$$+\mu_{j\to i}\left\{f_j N_j - \beta_j\left((N_j^2 + \sigma_j^2) + \alpha_{ji}(N_i N_j + C)\right)\right\}. \tag{A1.7}$$

Taking the limit $\Delta t \to 0$, and factoring N_i from the second term and N_j from the third term, we have

$$\frac{\mathrm{d}N_i}{\mathrm{d}t} = -\delta_i N_i + (1 - \mu_{i\to j})\left\{f_i - \beta_i\left(\left(N_i + \frac{\sigma_i^2}{N_i}\right) + \alpha_{ij}\left(N_j + \frac{C}{N_i}\right)\right)\right\} N_i$$
$$+\mu_{j\to i}\left\{f_j - \beta_j\left(\left(N_j + \frac{\sigma_j^2}{N_j}\right) + \alpha_{ji}\left(N_i + \frac{C}{N_j}\right)\right)\right\} N_j. \tag{A1.8}$$

The terms $N_i + \sigma_i^2/N_i$ and $N_j + C/N_i$ (and the two other similar terms) are more approachable if we allow $N_{j|i}$ to represent the expected number of individuals of genotype j in the patch of a randomly chosen individual of genotype i (rather than a randomly chosen patch). Eq. A1.6 can now be rewritten as $N_i N_{j|i} = E[q_i q_j] = N_i N_j + C$, and therefore $N_{j|i} = N_j + C/N_i$. Similarly, Eq. A1.5 yields $N_{i|i} = N_i + \sigma_i^2/N_i$. Using this notation, (A1.8) can be simplified to

$$\frac{\mathrm{d}N_i}{\mathrm{d}t} = -\delta_i N_i + (1 - \mu_{i\to j})\, F_i(N_{i|i}, N_{j|i})\, N_i + \mu_{j\to i}\, F_j(N_{j|j}, N_{i|j})\, N_j. \tag{A1.9}$$

From these equations we see that change in the first order moment (the expected density of genotype i) depends on second order moments (the variances and covariance of genotype densities). Thus, we now derive the dynamical equations for the change in these second order moments.

Variance Dynamics

Again, we consider a very small interval of time, Δt. The following holds:

$$\Delta q_i^2(t) = q_i^2(t + \Delta t) - q_i^2(t). \tag{A1.10}$$

Using (A1.1), (A1.2), (A1.3) and (A1.10), and again dropping the explicit time dependence in our notation, we see that

$$\Delta q_i^2 = (q_i - 1)^2 - q_i^2 = -2q_i + 1 \text{ with probability } P_i^-, \text{ and} \tag{A1.11}$$

$$\Delta q_i^2 = (q_i + 1)^2 - q_i^2 = 2q_i + 1 \text{ with probability } P_i^+. \tag{A1.12}$$

Thus, the expected change in q_i^2 is given by:

$$E[\Delta q_i^2] = E[(2q_i + 1)P_i^+ + (-2q_i + 1)P_i^-] \tag{A1.13}$$

We have the following relations:

$$E[q_i^3] = T_{iii} + 3N_i\sigma_i^2 + N_i^3, \tag{A1.14}$$

$$E\left[q_i^2 q_j\right] = T_{iij} + 2N_i C + N_j\sigma_i^2 + N_i^2 N_j, \tag{A1.15}$$

where T_{iii} and T_{iij} are the central third-order moments. Because of (A1.5), we also have

$$\frac{E[\Delta q_i^2]}{\Delta t} = \frac{\Delta N_i^2}{\Delta t} + \frac{\Delta \sigma_i^2}{\Delta t} \tag{A1.16}$$

Using (A1.5), (A1.6), (A1.14), (A1.15) and (A1.16), taking the limit $\Delta t \to 0$ and using the chain rule (i.e., $\frac{\mathrm{d}N_i^2}{\mathrm{d}t} = 2N_i \frac{dN_i}{\mathrm{d}t}$) , we have

$$\begin{aligned}\frac{\mathrm{d}\sigma_i^2}{\mathrm{d}t} = \frac{\mathrm{d}N_i}{\mathrm{d}t} &+ 2(N_i - \sigma_i^2)\delta_i \\ &+ 2(1 - m_i)\left(1 - \mu_{i\to j}\right)\left\{f_i\sigma_i^2 - \beta_i\left(T_{iii} + 2N_i\sigma_i^2 + \alpha_{ij}\left(T_{iij} + N_i C + N_j\sigma_i^2\right)\right)\right\} \\ &+ 2\left(1 - m_j\right)\mu_{j\to i}\left\{f_j C - \beta_j\left(T_{jji} + 2N_j C + \alpha_{ji}\left(T_{iij} + N_i C + N_j\sigma_i^2\right)\right)\right\}.\end{aligned} \tag{A1.17}$$

660 If we describe the third order moments exactly, we will find ourselves needing to describe fourth order
661 moments, which will in turn require fifth order moments, and so on. Here we use our moment closure
662 technique.
663
664 *Closing the Moments*
665 When migration is absolute (i.e., $m_i = m_j = 1$), the random variables q_i and q_j are
666 independently Poisson distributed among the patches with means equal to N_i and N_j, respectively (see
667 Neuhauser, 2002). For any independent Poisson-distributed random variables, their third order
668 moments can be described exactly in terms of lower-order moments; the homogeneous third central
669 moment is the corresponding first-order moment, while all mixed third central moments are zero:
670 $$T_{iii} = N_i$$
671 $$T_{iij} = 0$$
672 By using these substitutions as approximations when $m_i \approx m_j \approx 1$, we obviate the need to describe
673 higher order moments. This moment closure technique is exact when $m_i = m_j = 1$, and approximate
674 when $m_i \approx m_j \approx 1$.
675 Substituting our approximations for the third central moments into equation (A1.17), we have
676 $$\frac{\mathrm{d}\sigma_i^2}{\mathrm{d}t} = \frac{\mathrm{d}N_i}{\mathrm{d}t} + 2(N_i - \sigma_i^2)\delta_i$$
677 $$+ 2(1 - m_i)\big(1 - \mu_{i\to j}\big)\big\{f_i\sigma_i^2 - \beta_i\big(N_i + 2N_i\sigma_i^2 + \alpha_{ij}\big(N_iC + N_j\sigma_i^2\big)\big)\big\}$$
678 $$+2\big(1 - m_j\big)\mu_{j\to i}\big\{f_jC - \beta_j\big(2N_jC + \alpha_{ji}\big(N_iC + N_j\sigma_i^2\big)\big)\big\}. \qquad \text{(A1.18)}$$
679
680
681 *Covariance Dynamics*
682 Again, we consider a very small interval of time, Δt. The following holds:

$$\Delta\left(q_i(t)q_j(t)\right) = q_i(t+\Delta t)q_j(t+\Delta t) - q_i(t)q_j(t) \tag{A1.19}$$

Using, (A1.1), (A1.2), (A1.3) and (A1.16), and again dropping the explicit time dependence in our notations, we see that

$$\Delta(q_iq_j) = (q_i - 1)q_j - q_iq_j = -q_j \text{ with probability } P_i^-, \text{ and} \tag{A1.20}$$

$$\Delta(q_iq_j) = (q_i + 1)q_j - q_iq_j = q_j \text{ with probability } P_i^+. \tag{A1.21}$$

Thus, the expected change in the quantity q_iq_j is:

$$E\left[\Delta(q_iq_j)\right] = E\left[-q_jP_i^- - q_iP_j^- + q_jP_i^+ + q_iP_j^+\right]. \tag{A1.22}$$

From (A1.6), we have the following relation:

$$\frac{E[\Delta(q_iq_j)]}{\Delta t} = \frac{\Delta(N_iN_j)}{\Delta t} + \frac{\Delta C}{\Delta t}. \tag{A1.23}$$

Using (A1.5), (A1.6), (A1.14), (A1.15) and (A1.23), taking the limit $\Delta t \to 0$, and using the product rule (i.e., $\frac{\mathrm{d}(N_iN_j)}{\mathrm{d}t} = N_i\frac{\mathrm{d}N_j}{\mathrm{d}t} + N_j\frac{\mathrm{d}N_i}{\mathrm{d}t}$), we have

$$\begin{aligned}
\frac{\mathrm{d}C}{\mathrm{d}t} = {} & -(\delta_i + \delta_j)C + (1-m_i)(1-\mu_{i\to j})\left\{f_iC - \beta_i\left(\left(T_{iij} + 2N_iC\right) + \alpha_{ij}\left(T_{jji} + N_jC + N_i\sigma_j^2\right)\right)\right\} \\
& + (1-m_j)\mu_{j\to i}\left\{f_j\sigma_j^2 - \beta_j\left(\left(T_{jjj} + 2N_j\sigma_j^2\right) + \alpha_{ji}\left(T_{jji} + N_jC + N_i\sigma_j^2\right)\right)\right\} \\
& + (1-m_j)(1-\mu_{j\to i})\left\{f_jC - \beta_j\left(\left(T_{jji} + 2N_jC\right) + \alpha_{ji}\left(T_{iij} + N_iC + N_j\sigma_i^2\right)\right)\right\} \\
& + (1-m_i)\mu_{i\to j}\left\{f_i\sigma_i^2 - \beta_i\left(\left(T_{iii} + 2N_i\sigma_i^2\right) + \alpha_{ij}\left(T_{iij} + N_iC + N_j\sigma_i^2\right)\right)\right\}.
\end{aligned}$$

Substituting our approximations for the third central moments yields

$$\begin{aligned}
\frac{\mathrm{d}C}{\mathrm{d}t} = {} & -(\delta_i + \delta_j)C + (1-m_i)(1-\mu_{i\to j})\left\{f_iC - \beta_i\left(2N_iC + \alpha_{ij}\left(N_jC + N_i\sigma_j^2\right)\right)\right\} \\
& + (1-m_j)\mu_{j\to i}\left\{f_j\sigma_j^2 - \beta_j\left(\left(N_j + 2N_j\sigma_j^2\right) + \alpha_{ji}\left(N_jC + N_i\sigma_j^2\right)\right)\right\} \\
& + (1-m_j)(1-\mu_{j\to i})\left\{f_jC - \beta_j\left(2N_jC + \alpha_{ji}\left(N_iC + N_j\sigma_i^2\right)\right)\right\} \\
& + (1-m_i)\mu_{i\to j}\left\{f_i\sigma_i^2 - \beta_i\left(\left(N_i + 2N_i\sigma_i^2\right) + \alpha_{ij}\left(N_iC + N_j\sigma_i^2\right)\right)\right\}.
\end{aligned} \tag{A1.24}$$

With equations (A1.8), (A1.18) and (A1.24), we have a closed system of five differential equations describing the dynamics of N_W, N_M, σ_W^2, σ_M^2 and C.

Appendix 2: Equilibrium Densities

At equilibrium, $\frac{\mathrm{d}N_W}{\mathrm{d}t} = \frac{\mathrm{d}N_M}{\mathrm{d}t} = 0$. In this appendix, we assume $m_W = m_M = m$, $f_W = f_M = f$, $\beta_W = \beta_M = \beta$, $\alpha_{WM} = \alpha_{MW} = 1$, $\mu_{W\to M} = \mu$ and $\mu_{M\to W} = 0$. Using these assumptions and equation (A1.8), the equilibrium value $\widehat{N}_W$ must satisfy the following:

$$0 = -\delta_W \widehat{N}_W + (1-\mu)\{f\widehat{N}_W - \beta(\widehat{N}_W^2 + \hat{\sigma}_W^2 + \widehat{N}_W\widehat{N}_M + \hat{C})\}. \quad \text{(A2.1)}$$

If we assume that $m = 1$, then q_i and q_j are independently Poisson distributed, and therefore:

$$\hat{\sigma}_W^2 = \widehat{N}_W, \quad \text{(A2.2)}$$

$$\hat{C} = 0. \quad \text{(A2.3)}$$

Using (A2.2) and (A2.3), the non-zero equilibrium in (A2.1) is

$$\widehat{N}_W = \frac{(1-\mu)(f-\beta)-\delta_W}{(1-\mu)\beta} - \widehat{N}_M. \quad \text{(A2.4)}$$

We denote the total density at equilibrium $\hat{T} = \widehat{N}_W + \widehat{N}_M$. So, we have

$$\hat{T} = \frac{(1-\mu)(f-\beta)-\delta_W}{(1-\mu)\beta}, \quad \text{(A2.5)}$$

and

$$\widehat{N}_W = \hat{T} - \widehat{N}_M. \quad \text{(A2.6)}$$

Now we turn to the equilibrial density of the mutant genotype, $\widehat{N}_M$, again using (A1.8):

$$0 = -\delta_M \widehat{N}_M + \{f\widehat{N}_M - \beta(\widehat{N}_M^2 + \hat{\sigma}_M^2 + \widehat{N}_M\widehat{N}_W + \hat{C})\} + \mu\{f\widehat{N}_W - \beta(\widehat{N}_W^2 + \hat{\sigma}_W^2 + \widehat{N}_M\widehat{N}_W + \hat{C})\}. \quad \text{(A2.7)}$$

If we are assuming $m = 1$, the resulting Poisson distribution yields

$$\hat{\sigma}_M^2 = \widehat{N}_M, \quad \text{(A2.8)}$$

Using (A2.3), (A2.6), and (A2.8), the non-zero mutant equilibrium in (A2.7) is

$$\widehat{N}_M = \frac{-\mu\hat{T}(f-\beta(\hat{T}+1))}{-\delta_M+(1-\mu)(f-\beta(\hat{T}+1))}. \quad \text{(A2.9)}$$

After substituting, using (A2.5), and simplifying, equations (A2.4) and (A2.9) simplify to the following:

$$\widehat{N}_W = \frac{\{(1-\mu)\delta_M - \delta_W\}\{(f-\beta)(1-\mu)-\delta_W\}}{\beta(\delta_M-\delta_W)(1-\mu)^2}, \quad \text{(A2.10)}$$

$$\widehat{N}_M = \frac{\mu\delta_W\{(f-\beta)(1-\mu)-\delta_W\}}{\beta(\delta_M-\delta_W)(1-\mu)^2}. \quad \text{(A2.11)}$$

In order for $\widehat{N}_W$ and $\widehat{N}_M$ to be positive, we must have the following two conditions:

$$(1-\mu)(f-\beta) > \delta_W, \quad \text{(A2.12)}$$

$$(1-\mu)\delta_M > \delta_W. \quad \text{(A2.13)}$$

Note that (A2.13) is more stringent than the already assumed $\delta_M > \delta_W$. In all of what follows, we will assume conditions (A2.12) and (A2.13), except where explicitly mentioned. When $\mu = 0$, equations (A2.10) and (A2.11) simplify to:

$$\widehat{N}_W = \frac{f-\beta-\delta_W}{\beta}, \ \widehat{N}_M = 0, \quad \text{(A2.14)}$$

which gives a positive density of the wild type (by condition (A2.12)) and no mutant density. When $(1-\mu)\delta_M = \delta_W$ (i.e., right where equation (A2.13) starts to be violated), equations (A2.10) and (A2.11) simplify to:

$$\widehat{N}_W = 0, \ \widehat{N}_M = \frac{f-\beta-\delta_M}{\beta}, \quad \text{(A2.15)}$$

which gives a positive density of the mutant (by condition (A2.12), replacing δ_W with $(1-\mu)\delta_M$) and no wild-type density. Equilibria in (A2.14) and (A2.15) agree with single species equilibria from ecological models (Neuhauser, 2002; Pacala and Levin, 1997).

We let the fraction of mutants in the population be given by $\Phi(t)$, where

$$\Phi(t) = \frac{N_M(t)}{N_W(t)+N_M(t)}. \quad \text{(A2.16)}$$

Using equations (A2.10) and (A2.11), the mutation-selection balance under full migration is:

$$\widehat{\Phi} = \frac{\mu\delta_W}{(1-\mu)(\delta_M-\delta_W)}. \quad \text{(A2.17)}$$

Note that if $\mu = 0$, then $\widehat{\Phi} = 0$. That is, when there is no supply of new mutants through mutation, selection "wins" and no mutants remain at equilibrium; this corresponds to the special case of (A2.14). If $\mu = (\delta_M - \delta_W)/\delta_M$, then $\widehat{\Phi} = 1$. That is, as $\mu \to (\delta_M - \delta_W)/\delta_M$, mutation "wins" by overwhelming selection and only mutants remain at equilibrium; this corresponds to the special case of (A2.15).

Appendix 3: The Effect of Structure on Mutation-Selection Balance

In order to explore the role of structure on the mutant frequency, we look at

$$\frac{\partial \Phi}{\partial m} = \frac{\frac{\partial N_M}{\partial m} N_W - \frac{\partial N_W}{\partial m} N_M}{(N_W + N_M)^2}. \tag{A3.1}$$

Here we will evaluate $\left.\frac{\partial \Phi}{\partial m}\right|_{m=1}$. In order to do so, we must find $\left.\frac{\partial N_W}{\partial m}\right|_{m=1}$ and $\left.\frac{\partial N_M}{\partial m}\right|_{m=1}$, which we abbreviate with $\left.\frac{\partial N_W}{\partial m}\right|_1$ and $\left.\frac{\partial N_M}{\partial m}\right|_1$. To do this we differentiate (A1.8) with respect to m and evaluate at the $m = 1$ equilibrium. We start with equation (A1.8) where $i = W$.

$$0 = \{(1-\mu)[f - \beta(2\widehat{N}_W + \widehat{N}_M)] - \delta_W\}\left.\frac{\partial N_W}{\partial m}\right|_1 - \{\beta(1-\mu)\widehat{N}_W\}\left.\frac{\partial N_M}{\partial m}\right|_1 - \{\beta(1-\mu)\}\left.\frac{\partial \sigma_W^2}{\partial m}\right|_1 - \{\beta(1-\mu)\}\left.\frac{\partial C}{\partial m}\right|_1. \tag{A3.2}$$

Again, we see that we will need to consider partial derivatives of higher-order moments with respect to m to solve (A3.1). By differentiating equations (A1.8) with $i = M$, (A1.18) with $i = W$, (A1.18) with $i = M$, and (A1.24), all with respect to m and making the appropriate substitutions for when $m = 1$, we obtain other equalities involving partial derivatives (similar to (A3.2)). This leads to the following linear system:

$$\mathbf{A}\vec{\partial}_1 = \vec{c}, \tag{A3.3}$$

where,

$$\mathbf{A} = \begin{bmatrix} (1-\mu)\{f - \beta(2\widehat{N}_W + \widehat{N}_M)\} - \delta_W & -\beta(1-\mu)\widehat{N}_W & -\beta(1-\mu) & 0 & -\beta(1-\mu) \\ -\beta(1+\mu)\widehat{N}_M + \mu(f - 2\beta\widehat{N}_W) & f - 2\beta\widehat{N}_M - \beta(1+\mu)\widehat{N}_W - \delta_M & -\beta\mu & -\beta & -\beta(1+\mu) \\ \delta_W & 0 & -\delta_W & 0 & 0 \\ 0 & \delta_M & 0 & -\delta_M & 0 \\ 0 & 0 & 0 & 0 & -\delta_W - \delta_M \end{bmatrix},$$

767 $$\vec{\partial}_1 = \begin{bmatrix} \left.\frac{\partial N_W}{\partial m}\right|_1 \\ \left.\frac{\partial N_M}{\partial m}\right|_1 \\ \left.\frac{\partial \sigma_W^2}{\partial m}\right|_1 \\ \left.\frac{\partial \sigma_M^2}{\partial m}\right|_1 \\ \left.\frac{\partial C}{\partial m}\right|_1 \end{bmatrix}, \text{ and } \vec{c} = \begin{bmatrix} 0 \\ 0 \\ \widehat{N}_W(1-\mu)\{f-\beta(1+2\widehat{N}_W+\widehat{N}_M)\} \\ \widehat{N}_M\{f-\beta(1+2\widehat{N}_M+(1+\mu)\widehat{N}_W)\} \\ \widehat{N}_W\{\mu(f-\beta(1+2\widehat{N}_W))-2\beta\widehat{N}_M\} \end{bmatrix}.$$

768 Solving system (A3.3) and using $\left.\frac{\partial N_W}{\partial m}\right|_1$ and $\left.\frac{\partial N_M}{\partial m}\right|_1$ for equation (A3.1) gives the following:

769 $$\left.\frac{\partial \Phi}{\partial m}\right|_{m=1} = -\frac{\beta\mu}{(1-\mu)^2\delta_M\{(\delta_M/\delta_W)^2-1\}}. \quad \text{(A3.4)}$$

770 We abbreviate $\left.\frac{\partial \Phi}{\partial m}\right|_{m=1}$ as $\partial_m\Phi$. From equation (A3.4), it is not difficult to show that $\frac{\partial|\partial_m\Phi|}{\partial\beta} > 0$,

771 $\frac{\partial|\partial_m\Phi|}{\partial\mu} > 0$, $\frac{\partial|\partial_m\Phi|}{\partial\delta_M} < 0$, and $\frac{\partial|\partial_m\Phi|}{\partial\delta_W} > 0$. That is, as the competition coefficient β, the mutation rate μ,

772 or the death rate of the wild type genotype increase, the addition of structure to an unstructured system

773 leads to a greater increase in the mutant class frequency. As the death rate of the mutant is increased,

774 the addition of structure to an unstructured system leads to a smaller increase in the mutant class

775 frequency.

776

777 ***Appendix 4: Gillespie Algorithm***

778 Our simulation is based on a Gillespie algorithm (Gillespie, 1977) that we coded in the Python

779 2.7 scripting language. The Gillespie algorithm simulates a possible trajectory of a continuous time

780 stochastic system.

781 In our system of *P* connected patches, patches must be initialized before simulating evolution.

782 Unless otherwise indicated, we seeded our patches with wild-type and mutant individuals by

783 repeatedly drawing from independent Poisson distributions whose parameters are the full migration

784 equilibria $\widehat{N}_W$ and $\widehat{N}_M$ from (A2.10) and (A2.11), respectively. The initial population defines update

zero, for which the time variable t is also zero. As the populations are seeded from their corresponding $m = 1$ equilibrium distributions, structure is introduced as any limited migration simulation begins.

Evolution of the population occurs over "update" steps. First, for update u each patch p receives four "weights", corresponding to the four possible events in that patch: a wild-type birth, a mutant birth, a wild-type death, and a mutant death. Each event's weight is proportional to its rate. If we let the number of genotypes W and M in a patch p at update step u be given by $n_W(u,p)$ and $n_M(u,p)$, respectively, then the weights are defined as follows:

$$k_1(u,p) = f n_W(u,p) - \beta n_W(u,p)\big(n_W(u,p) + n_M(u,p)\big), \tag{A4.1}$$

$$k_2(u,p) = f n_M(u,p) - \beta n_M(u,p)\big(n_W(u,p) + n_M(u,p)\big), \tag{A4.2}$$

$$k_3(u,p) = \delta_W n_W(u,p), \tag{A4.3}$$

$$k_4(u,p) = \delta_M n_M(u,p). \tag{A4.4}$$

The event that is attempted at update step u is either a death, a birth with migration, or a birth without migration, and the decision is made stochastically using the following weights:

$$K_{death}(u) = \sum_{p=1}^{P} k_3(u,p) + \sum_{p=1}^{P} k_4(u,p), \tag{A4.5}$$

$$K_{birth\_mig}(u) = m\Big\{\sum_{p=1}^{P} k_1(u,p) + \sum_{p=1}^{P} k_2(u,p)\Big\}, \tag{A4.6}$$

$$K_{birth\_natal}(u) = (1-m)\Big\{\sum_{p=1}^{P} |k_1(u,p)| + \sum_{p=1}^{P} |k_2(u,p)|\Big\}. \tag{A4.7}$$

Time increment Δt is drawn from an exponential distribution whose rate is equal to $K_{death}(u) + K_{birth\_mig}(u) + K_{birth\_natal}(u)$, and time parameter t is incremented to $t + \Delta t$. For Figure 2 and Supplementary Figure 1, the time increment's exponential distribution rate is equal to $k_1 + k_2 + k_3 + k_4$, which does not noticeably affect the resulting time steps.

The $K_{birth\_natal}(u)$ terms are summed using absolute values due to potentially negative intra-patch birth rates. Since birth rates decrease linearly with density, $k_1(u,p)$ and $k_2(u,p)$ may be negative occasionally in particularly crowded patches. For migrating events, the negative births reduce

the mean birth rate, which was never negative for the conditions of our simulations. For non-migrating births, a negative birth event decrements, rather than increments, the chosen genotype population in a patch. Thus, for any patch r, if a non-migrating birth event is chosen:

$$n_W(u+1,r) = n_W(u,r) + \text{sgn}(k_1(u,r)) \text{ with probability } (1-\mu)\frac{|k_1(u,r)|}{K_{birth\_natal(u)}}, \quad \text{(A4.8)}$$

$$n_M(u+1,r) = n_M(u,r) + \text{sgn}(k_2(u,r)) \text{ with probability } \frac{|k_2(u,r)|}{K_{birth\_natal}(u)} + \mu\frac{|k_1(u,r)|}{K_{birth\_natal}(u)}, \quad \text{(A4.9)}$$

If a migrating birth event is chosen (i.e., a migrant will 'land' on a random patch):

$$n_W(u+1,r) = n_W(u,r) + 1 \text{ with probability } \frac{1-\mu}{P}\sum_{p=1}^{P}\frac{k_1(u,p)}{K_{birth\_mig}(u)}, \quad \text{(A4.10)}$$

$$n_M(u+1,r) = n_M(u,r) + 1 \text{ with probability } \frac{1}{P}\left\{\sum_{p=1}^{P}\frac{k_2(u,p)}{K_{birth\_mig}(u)} + \mu\sum_{p=1}^{P}\frac{k_1(u,p)}{K_{birth\_mig}(u)}\right\}, \quad \text{(A4.11)}$$

If a death event is chosen:

$$n_W(u+1,r) = n_W(u,r) - 1 \text{ with probability } \frac{k_3(u,r)}{K_{death}(u)}, \quad \text{(A4.12)}$$

$$n_M(u+1,r) = n_M(u,r) - 1 \text{ with probability } \frac{k_4(u,r)}{K_{death}(u)} \quad \text{(A4.13)}$$

Simulations were run for 200,000 updates (for $1 \geq m \geq 0.95$), 500,000 updates (for $0.95 > m \geq 0.7$), or 1,000,000 updates (for $0.7 > m > 0$). Data was recorded every 5000 updates, and equilibrial values represent a simulation's average state over its final 10,000 updates.

Acknowledgements

The authors thank Michael Whitlock and Ruth Shaw for their helpful comments, and Jacob Speidel, Brian Connelly, and Joshua Nahum for their coding help. The authors are also grateful to the anonymous reviewers for their many useful suggestions. This work was supported in part by the National Science Foundation Graduate Research Fellowship under grants DGE-0718124 and DGE-1256082, as well as NSF Cooperative Agreement DBI-0939454 and an NSF CAREER Award (DEB0952825).

Chapter 2

Evolution at 'sutures' and 'centers':
Recombination can aid adaptation of spatially structured populations on rugged fitness landscapes

Jacob D Cooper[*,†] & Benjamin Kerr[*,†]

[*] *Department of Biology, University of Washington, Seattle, WA*

[†] *BEACON Center for the Study of Evolution in Action, University of Washington, Seattle, WA*

Running title:

Evolution at ‘sutures’ and ‘centers’

Corresponding author:

Jacob D Cooper

University of Washington

Department of Biology

Box 351800

Seattle, WA 98195-1800

phone: (206) 221-7026

email: yankel@uw.edu

Keywords:

recombination

spatial structure

rugged fitness landscapes

peak-jumping

Abstract:

Epistatic interactions among genes can give rise to rugged fitness landscapes, in which multiple "peaks" of high-fitness allele combinations are separated by "valleys" of low-fitness genotypes. How populations traverse rugged fitness landscapes is a long-standing question in evolutionary biology. Sexual reproduction may affect how a population moves within a rugged fitness landscape. Sex may generate new high-fitness genotypes by recombination, but it may also destroy high-fitness genotypes by shuffling the genes of a fit parent with a genetically distinct mate, creating low-fitness offspring. Either of these opposing aspects of sex require genotypic diversity in the population. Spatially structured populations may harbor more diversity than well-mixed populations, potentially amplifying both positive and negative effects of sex. On the other hand, spatial structure leads to clumping in which mating is more likely to occur between like types, diminishing the effects of recombination. In this study, we use computer simulations to investigate the combined effects of recombination and spatial structure on adaptation in rugged fitness landscapes. We find that spatially restricted mating and offspring dispersal may allow multiple genotypes inhabiting suboptimal peaks to coexist, and recombination at the "sutures" between the clusters of these genotypes can create genetically novel offspring. Sometimes such an offspring genotype inhabits a new peak on the fitness landscape. In such a case, spatially restricted mating allows this fledgling subpopulation to avoid recombination with distinct genotypes, as mates are more likely to be the same genotype. Such population "centers" can allow nascent peaks to establish despite recombination. Spatial structure may therefore allow an evolving population to enjoy the creative side of sexual recombination while avoiding its destructive side.

Author Summary:

For a novel genotype to establish in a population, it must (1) be created, and (2) not be subsequently lost. Recombination is a double-edged sword in this process, potentially fostering creation, but also hastening loss as the novel genotype is being recombined with other genotypes, especially when rare. In this study, we find that spatial structure may affect both the creative and destructive aspects of recombination in rugged fitness landscapes. By slowing the spread of high-fitness genotypes, spatially restricted mating and dispersal may allow diverse subpopulations to arise. Reproduction across the borders of these subpopulations—at "sutures"—may create genetic novelty. Depending on the topography of the fitness landscape, such novelty may be in the domain of attraction of a new, higher peak; the population may "peak-jump" to an area of genotype space unlikely to be explored by mutation alone. Lineages founded by peak-jumping events are particularly prone to early extinction, as recombination with unlike genotypes may disrupt the rare allele combination and thereby produce low-fitness offspring. However, these fledgling peak lineages may be protected from early extinction by mating within small homotypic clusters—in "centers". Thus, spatial structure may allow a population to create rare genotypes via recombination, and allow those rare genotypes to persist *despite* recombination.

967 **Introduction**

968 Sexual recombination has long been a puzzling evolutionary strategy (see [1,2]). Recombination has
969 the potential to create novel high-fitness genotypes in a population, but also to destroy high-fitness
970 lineages by recombining them with genetically distinct lineages. Whether recombination speeds or
971 slows adaptation depends largely on the relative strengths of its creative and destructive effects.
972
973 One of the earliest adaptive explanations for recombination is the Fisher-Muller effect, in which
974 beneficial alleles in different lineages can recombine into a single lineage, speeding adaptation [3,4].
975 The Fisher-Muller effect exemplifies the creative aspect of sex, and many studies have shown faster
976 adaptation due to Fisher-Muller dynamics [5–8]. However, the Fisher-Muller effect assumes that
977 beneficial alleles remain beneficial when recombined into new genetic backgrounds. This assumption
978 is necessarily broken in multi-peaked fitness landscapes [9], which arise when genetic interactions
979 among loci yield multiple high-fitness allele combinations separated by valleys of low-fitness
980 intermediate genotypes. In such landscapes, the adaptive effects of recombination are more complex.
981
982 Studies on two-locus rugged landscapes focus on escape from suboptimal peaks, and have found that
983 modest levels of recombination may speed adaptation slightly, while substantial recombination slows
984 or halts adaptation entirely [10–12]. However, studies on rugged landscapes with more than two loci
985 yield conflicting results, variously reporting recombination as slowing adaptation [13], speeding
986 adaptation [14], or having complex effects dependent on the topography of a fitness landscape, the
987 population inhabiting it, and the time scale considered [15–17]. Studies on empirical fitness landscapes
988 report recombination as speeding adaptation [6,18] or having complex effects dependent on the fitness
989 topography and rate of recombination [15]. The varied results described above may partly depend on

990 the genetic variation that a particular landscape supports. If there are multiple suboptimal peak
991 genotypes, these competing lineages may interact. Depending on the topography of the fitness
992 landscape, recombination between individuals on different suboptimal peaks may create an offspring
993 in the attractive domain of a novel peak, termed "peak-jumping" [15,19]. Thus, in topographies that
994 permit peak-jumping, when *sub*populations occupy different suboptimal peaks, recombination may
995 allow peak-jumping to novel, higher peaks.
996
997 What conditions might enable a recombining population to maintain the diversity required for peak-
998 jumping? Restricted mating and dispersal (which we call "local reproduction") may promote
999 population-wide diversity by slowing the spread of high-fitness genotypes and creating competitive
1000 refugia for lower-fitness genotypes [20,21]. However, the same spatial restriction that allows
1001 population-wide diversity also impedes recombination between those diverse types, as mating occurs
1002 largely within monotypic clusters. Martens and Hallatschek [21] show that recombination between
1003 spatially abutting lineages (which we call "sutures") can be sufficient to speed adaptation due to
1004 Fisher-Muller effects in their smooth landscape model. In some rugged landscapes, recombination at
1005 sutures may allow peak-jumping. However, lineages founded by peak-jumping events are particularly
1006 prone to early extinction as recombination may disrupt the rare allele combinations and consequently
1007 prevent establishment—recombination with the majority genotype may pull fledgling peak populations
1008 off their precipices and into the valley between [22]. On the other hand, recombination within
1009 monotypic clusters (which we call "centers") may allow high fidelity of rare allele combinations, but
1010 also prevent the creation of such rare allele combinations as no effective recombination is occurring.
1011 Which effects of sutures and centers dominate, and in what circumstances? In this paper, we examine
1012 the combined effects of recombination and local reproduction on adaptation on rugged landscapes.

Model

In our simulation, a population inhabits an $L \times L$ regular square lattice with wraparound edges (a toroid). Each lattice point may be empty or may house one organism. Organisms have a haploid genotype of N loci, where the allele at each locus is either a 0 or a 1. Each genotype has an associated survival probability (s_G). Populations are initialized with individuals of the genotype farthest from the optimal genotype (that is, G_0 such that $H(G_0, G_{opt}) = N$, where H is the Hamming distance operator and G_{opt} is the optimal genotype), unless otherwise indicated. Evolution occurs via discrete update steps described below, and simulations conclude when the optimal genotype reaches a predefined frequency, or when a predefined number of epochs have occurred, where an epoch is defined as $L \times L$ updates.

At each update, a point is chosen at random. If this focal point houses an individual of genotype G, the individual dies with probability $1 - s_G$, and the lattice point becomes empty. If the focal point is already empty, then a birth event can occur. For a birth event, two parents are needed. The first parent is chosen from a pre-defined dispersal neighborhood about the focal point, and second parent is chosen from a pre-defined mating neighborhood about the first parent. For simplicity, we set the sizes of these two neighborhoods equal, and call the radius of this neighborhood the "reproductive distance". We focus on two extreme cases. In our "local reproduction" condition, a focal point's neighborhood is defined by the lattice points immediately to the north, east, south and west (the Von Neumann neighborhood); in our "global reproduction" condition, the neighborhood is defined as the entire lattice, minus the focal point.

Once the parents are chosen, an offspring genotype is formed by recombination and mutation. To simulate recombination, one of the two parents is chosen at random to contribute the allele at the first locus, and between-locus crossover occurs with probability r. Thus $r = 0$ yields no crossing over, while $r = 0.5$ yields independent assortment of parental alleles. To simulate mutation, each locus of the recombined offspring's binary genotype changes its allelic state (0→1 or 1→0) with probability μ. Finally, the offspring is born, and inhabits the initially-empty lattice point.

Results and Discussion

To investigate the interplay of recombination and reproductive distance, we use a 4x2 factorial design: four recombination probabilities and two neighborhood sizes. For each factorial combination, we simulate replicate populations evolving on a multi-peaked rugged landscape. Our default fitness landscape is defined to allow peak-jumping; that is, there exist two suboptimal peaks (0011 and 1100) which can recombine to produce the optimal genotype (1111). We will relax this contrivance later in our results. In our 4x2 experiment, all populations are initialized on a suboptimal peak (0000), and all parameters (lattice size, initial density, mutation rate, *etc*.) are held constant for all simulations. We find that the qualitative effect of recombination – whether it speeds or slows the traversal of the rugged fitness landscape – can depend on whether reproduction is localized (Figure 1), and this interaction between recombination and reproductive neighborhood is significant ($p<0.001$, Manly's permutation test [23]). When reproduction is global, recombination never speeds, and can even slow, peak establishment. Conversely, when reproduction is local, recombination never slows but can speed peak establishment.

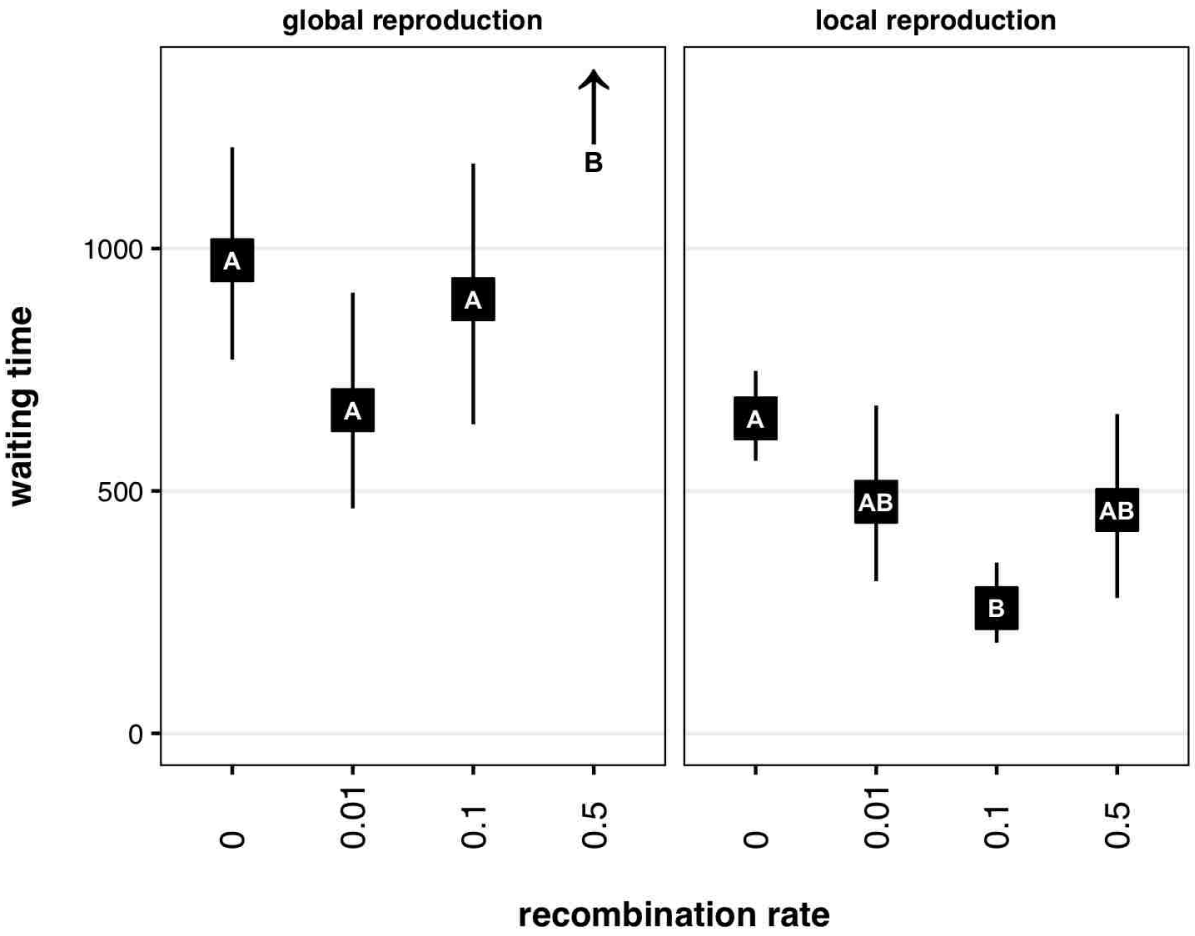

Figure 1. Waiting time to establishment of an optimal peak genotype at various recombination rates. We define establishment as discovery without subsequent extinction, and time as simulation epochs (see Methods). Data points and error bars represent mean values and standard error of 75 replicate simulations using parameter values $L = 70$, $\mu = 0.002$, $s_G = 0.2$, $s_{0000} = 0.6$, $s_{1100} = s_{0011} = 0.85$, $s_{1111} = 0.9$, where G represents all non-specified genotypes. Within each reproductive distance, data points with no shared letter are significantly different (Tukey's HSD, $\alpha = 0.05$). The upward arrow indicates that establishment never occurred by the simulation maximum of 2000 epochs.

To investigate why the effect of recombination may depend on reproductive distance, we focus on two aspects of a genotype's spread through a population: discovery and establishment. For a peak genotype to establish in a population, it must (1) be created, and (2) not be subsequently lost.

Local reproduction fosters the creation of novel genotypes via recombination

On rugged fitness landscapes, populations may become trapped on a suboptimal fitness peak. It is also possible for a population to discover multiple distinct suboptimal peaks before any single peak genotype has fixed. Localized reproduction may promote the coexistence of multiple peaks by increasing the time-to-fixation of a newly discovered peak. Thus, localized reproduction may foster the diversity of genotypes required for peak-jumping via recombination (*e.g.*, the creation of peak genotype 1111 due to recombination between suboptimal peak genotypes 0011 and 1100). However, localized reproduction precludes peak-jumping unless the peak lineages are physically close. Physical proximity could result if two expanding peak lineages eventually abut, allowing meaningful recombination at the suture between the distinct genotypes. Such sutures between subpopulations may allow repeated discovery of genotypes in the domain of attraction of a higher fitness genotype. Indeed, in a representative simulation of intermediate recombination with local reproduction from Figure 1, multiple suboptimal peak genotypes coexist (0011 and 1100), and the globally optimal genotype (1111) is repeatedly created at the sutures between these subpopulations (Figure 2B, supplemental video). In a parallel representative run with global reproduction, no such sutures exist, because an intermediate genotype, once discovered, quickly sweeps to near fixation (Figure 2A, supplemental video).

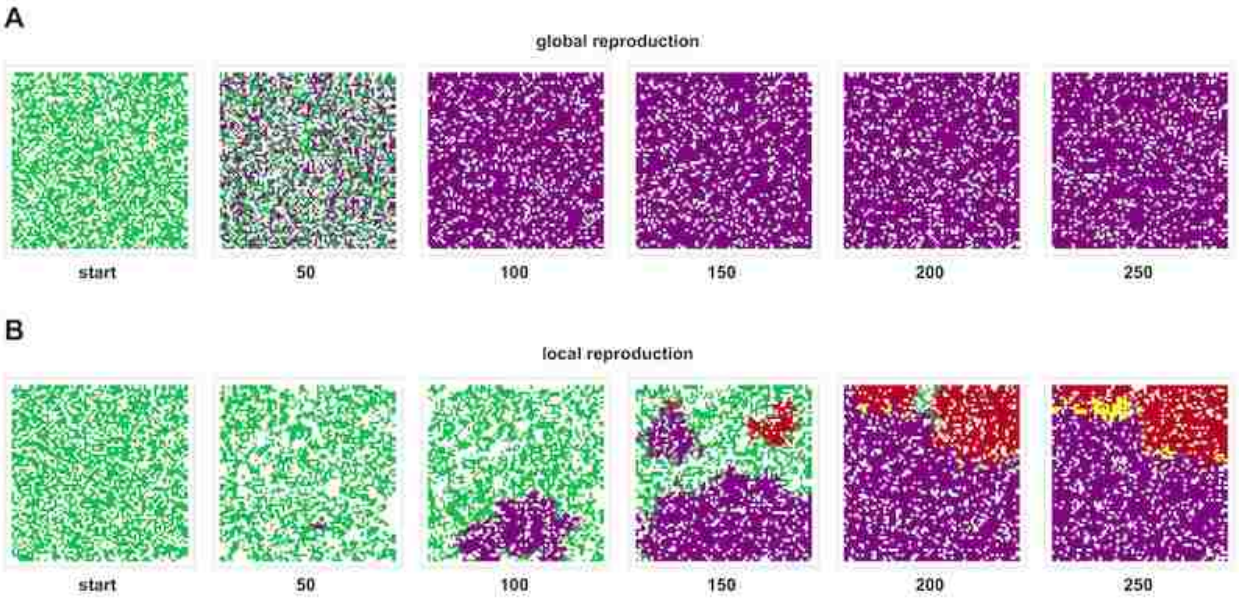

Figure 2. Population snapshots of representative runs from Figure 1 with a recombination rate between adjacent loci of 0.1. When reproduction is global (A), a suboptimal peak (purple) fixes by epoch 100, rendering recombination ineffective. When reproduction is local (B), two suboptimal peaks (purple and red) exist by epoch 150, and these subpopulations expand to physical proximity by epoch 200. The optimal genotype (yellow) is then created multiple times via peak-jumping at the suture between the two suboptimal peaks.

Does local reproduction encourage sutures between subpopulations? To test this, we simulate a two-locus landscape with two peak genotypes (10 and 01) and two valley genotypes (00 and 11, the latter of which is lethal). The population is initialized on genotype 00, and we track how frequently genotype 11 is created, and how it is created. We find that genotype 11 is created by recombination more frequently in local rather than global reproductive schemes, while it is created by mutation at approximately the same frequency in the two schemes (Supplemental Figure 1).

Local reproduction mitigates the loss of novel genotypes via recombination

Once a peak genotype is discovered, it may be lost due to subsequent recombination with unlike types, lowering the genotypic fidelity of its lineage. When recombination rates are high, such loss may prevent a genotype from establishing. However, spatially segregated populations may harbor population "centers", in which mating pairs are likely to be genetically similar, preserving genotypic fidelity. Such centers may allow rare genotypes to persist in a population despite recombination. To examine the effect of centers on the establishment of a novel peak genotype, we model adaptation on a two-locus landscape in which a population may escape from suboptimal peak genotype 00 by crossing an adaptive valley (genotypes 10 and 01) to optimal peak genotype 11. We find a three-way interaction between recombination, reproductive distance, and centers ($p=0.03$, Manly's permutation test). Frequent recombination slows the establishment of the optimal peak genotype in global but not local reproductive schemes (Figure 3, top row). However, if optimal peak genotypes are prohibited from mating with each other when rare (*i.e.*, when they comprise less than 1% of the population), the local and global reproductive schemes have similar results when recombination is frequent (Fig 3, bottom row).

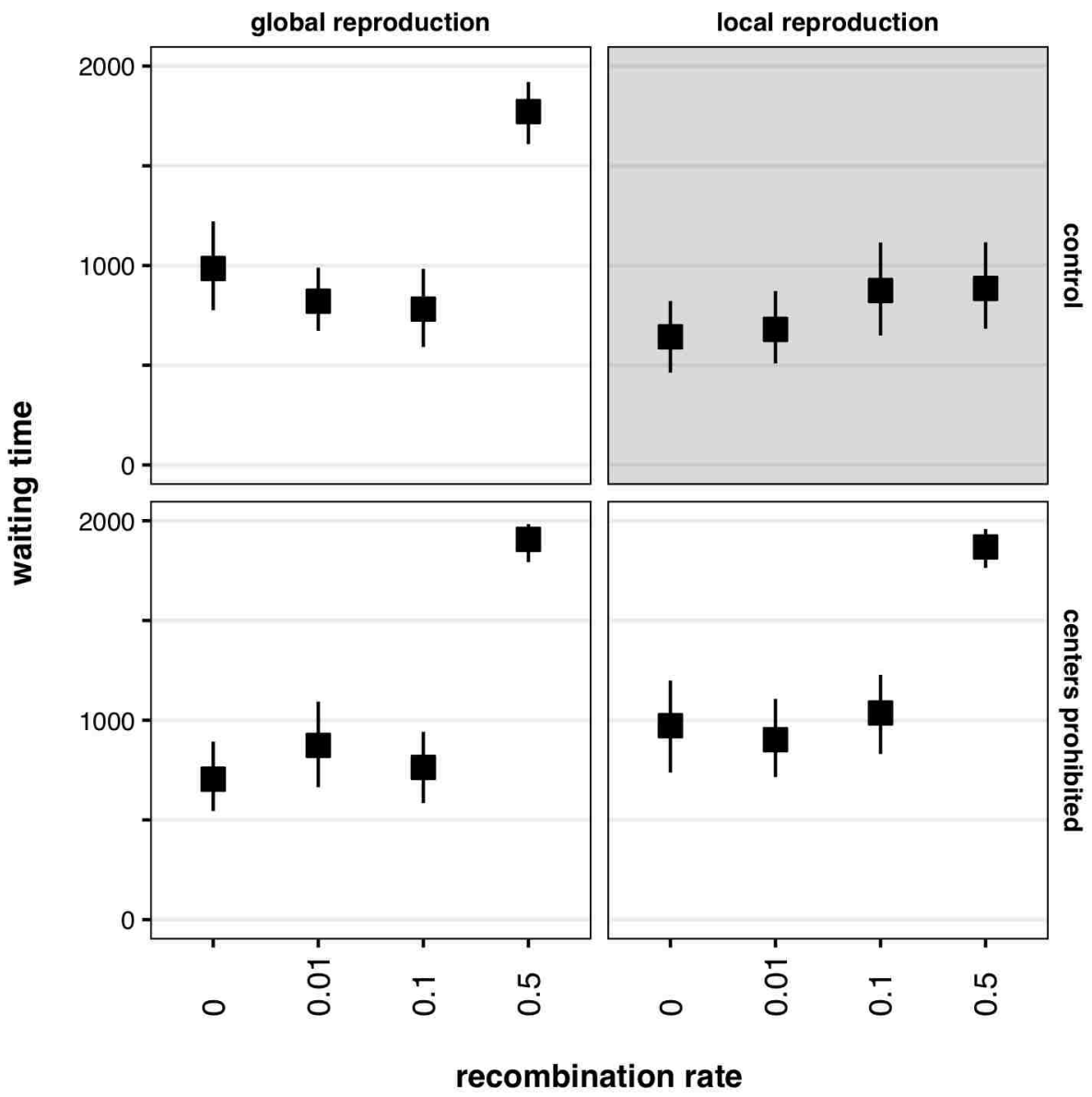

Figure 3. Waiting time to establishment of an optimal peak genotype at various recombination rates, with and without prohibiting "centers". Populations are initialized on suboptimal peak genotype 00, and must cross an adaptive valley to optimal peak genotype 11. Clustered genotype centers allow nascent peaks to establish despite frequent recombination. When reproduction is global, frequent recombination prevents valley-crossing. Likewise, when genotype 11 individuals are prohibited from mating with each other until they have reached a frequency of 1% ("centers prohibited" treatments), frequent recombination prevents valley-crossing. However, local reproduction with naturally occurring clusters of rare genotypes ("centers") allows valley-crossing even with frequent recombination (top-right, shaded). Data points and error bars represent mean values and standard error of 40 replicate simulations using parameter values $L = 70$, $\mu = 0.001$, $s_{00} = 0.8$, $s_{10} = s_{01} = 0.6$, $s_{11} = 0.9$.

While recombination may allow a population to more quickly climb a local peak, it can also trap populations on suboptimal peaks [17]. However, recombination may aid escape from suboptimal peaks if the landscape topography supports a diversity of genotypes and permits peak-jumping [14,19,24]. Sutures should be most effective when recombination between two suboptimal peaks can create offspring in the attraction basin of a third, higher peak, allowing for peak-jumping. Centers should be most effective when novel peaks are discovered via peak-jumping, as recombination between the nascent peak and the majority genotypes can create low-fitness offspring. Thus the ability of sutures and centers to modulate the effects of recombination—to harness the creative aspect and mitigate the destructive aspect—may be sensitive to the particular topography of a rugged landscape.

Sutures and centers in empirically derived fitness landscapes

The full topographies of some naturally occurring fitness landscapes have been measured for small subsets of their genotype spaces [25]. De Visser *et al.* [15] generated 5-locus empirical fitness landscapes by introducing deleterious mutations into the asexual fungus *A. niger*, and measuring the fitness effects of five individual mutations and all combinations thereof. Two complete 5-locus fitness landscapes were generated, with 32 genotypes each (though the landscapes are not completely independent as they share four of their five loci of interest). Both landscapes were found to be rugged, with multiple local maxima and minima. However, only one of the landscapes (which we call PJ^+) had suboptimal peaks which could recombine into the attraction basin of the optimal peak; the other landscape (PJ^-) did not. De Visser *et al.* found that recombination generally slows or halts the establishment of the optimal genotype in either landscape, though there was a window of very infrequent recombination that could speed adaptation in PJ^+ and very slightly and rarely speed adaptation in PJ^- (see [15], supplement B1). We create landscapes parallel to PJ^+ and PJ^- for our model

(*e.g.*, replacing relative fitness with relative survival probabilities), and simulate evolution as before. We find a significant three-way interaction between recombination, reproductive distance, and fitness landscape topology on the waiting time for optimal genotype establishment ($p<0.001$, Manly's permutation test). On PJ^{+}, recombination slows or prevents the establishment of the optimal genotype when reproduction is global, but never slows or prevents adaptation when reproduction is local. On PJ^{-}, whose topography is less conducive to landscape exploration via recombination, we find similar results to PJ^{+} when reproduction is global, but high recombination ($r=0.5$) still slows the generation and establishment of the optimal genotype when reproduction is local.

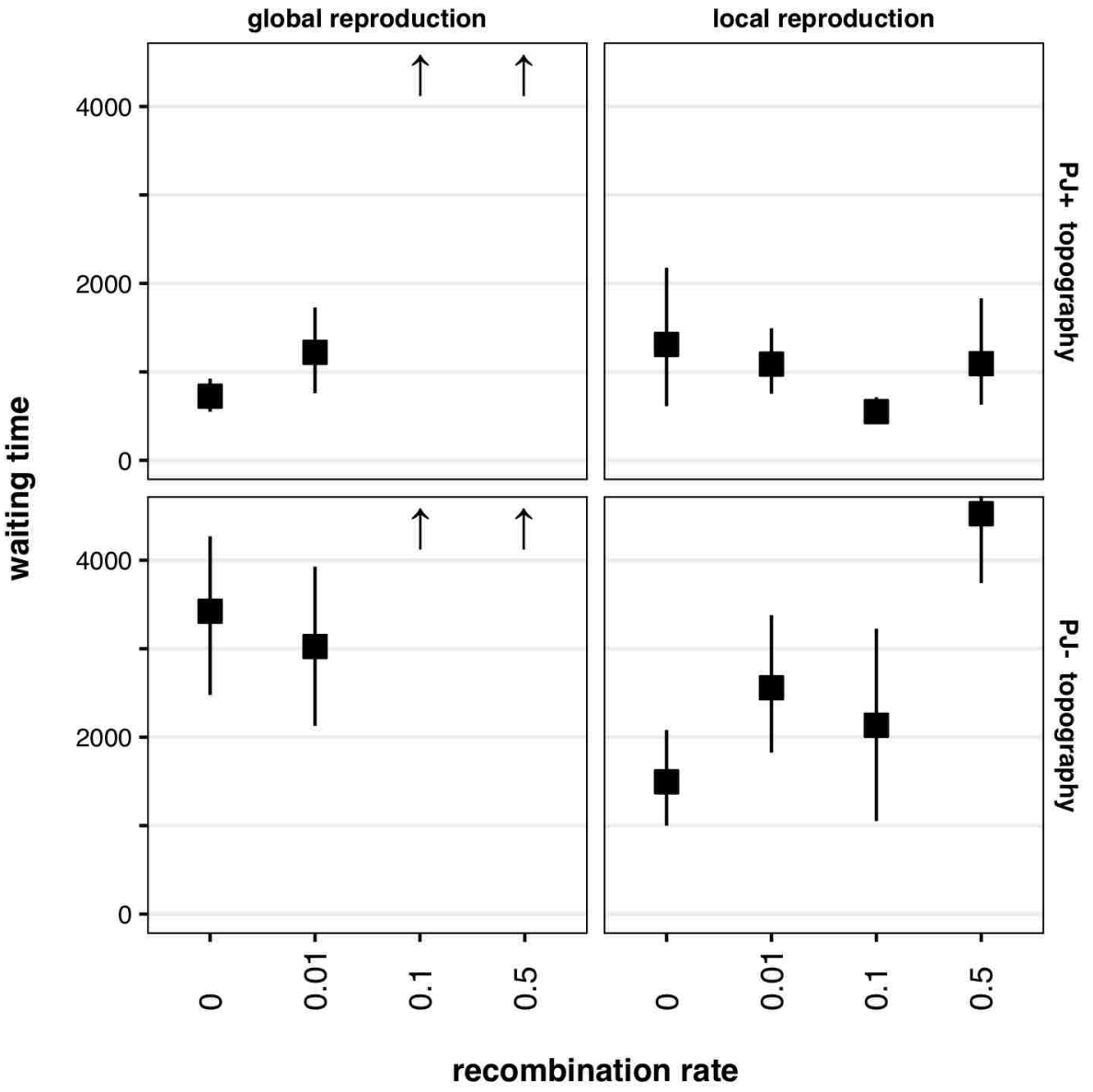

Figure 4. Waiting time to establishment of optimal genotypes on empirically-derived rugged landscapes at various recombination rates. When reproduction is global, recombination slows or prevents the establishment of an optimal genotype (left column). Local reproduction mitigates the slowing effect of recombination in both landscapes. In the landscape whose topography allows recombination between suboptimal peaks to create an offspring in the attractive basin of the optimal genotype—a landscape that permits peak-jumping—recombination can speed the establishment of the optimal genotype (top-right panel). Data points and error bars represent mean values and standard error of 15 replicate simulations using parameter values $L = 70$, $\mu = 0.001$. Upward arrows indicate that establishment never occurred by the simulation maximum of 5000 epochs. For an explanation of the conversion from relative fitnesses (as reported in [15] to comparable survival probabilities (as used in this model), see Appendix.

In our test landscape and in two empirically-derived landscapes, sufficiently high rates of recombination prohibit the establishment of a novel high-fitness peak when reproduction is global, but this destructive side of recombination is alleviated when reproduction is local. Moreover, in landscape topographies that allow peak-jumping (our test landscape and, to a lesser extent, PJ^{+}), recombination can speed the establishment of novel high-fitness peaks. Thus, the landscape topography affects the ability of local reproduction to mediate the effects of recombination: accentuating exploration via "sutures" while mitigating recombinatory destruction of rare genotypes via "centers". We suggest the greatest effect of sutures occurs when peak-jumping is possible, and the greatest effect of centers occurs when novel peaks are created via peak-jumping. Indeed, we see an amplified effect of local reproduction on a contrived fitness landscape with six suboptimal peaks and many opportunities for peak-jumping (Supplemental Figure 2). The prevalence of such topographical features and spatial restrictions—and therefore how relevant "sutures" and "centers" are to natural populations—remains an empirical question. It is possible, though, that by creating "sutures", spatially structured populations may efficiently explore rugged landscapes via recombination, and by creating "centers", those same populations may permit the establishment of novel peaks *despite* recombination. Spatially structured populations may therefore harness recombination's constructive effects while mitigating its destructive effects on adaptation in rugged landscapes.

References

1. Otto SP, Lenormand T. Resolving the paradox of sex and recombination. Nat Rev Genet. 2002;3: 252–261. doi:10.1038/nrg761
2. Otto SP, Gerstein AC. Why have sex? The population genetics of sex and recombination. Biochemical Society Transactions. 2006;34: 519–522. doi:10.1042/BST0340519
3. Fisher RA. The Genetical Theory of Natural Selection: A Complete Variorum Edition. OUP Oxford; 1930.
4. Muller HJ. Some Genetic Aspects of Sex. The American Naturalist. 1932;66: 118–138.
5. Christiansen FB, Otto SP, Bergman A, Feldman MW. Waiting with and without recombination: the time to production of a double mutant. Theor Popul Biol. 1998;53: 199–215. doi:10.1006/tpbi.1997.1358
6. Colegrave N. Sex releases the speed limit on evolution. Nature. 2002;420: 664–666.
7. Cooper TF. Recombination Speeds Adaptation by Reducing Competition between Beneficial Mutations in Populations of Escherichia coli. PLOS Biol. 2007;5: e225. doi:10.1371/journal.pbio.0050225
8. McDonald MJ, Rice DP, Desai MM. Sex speeds adaptation by altering the dynamics of molecular evolution. Nature. 2016;531: 233–236. doi:10.1038/nature17143
9. Poelwijk FJ, Tănase-Nicola S, Kiviet DJ, Tans SJ. Reciprocal sign epistasis is a necessary condition for multi-peaked fitness landscapes. Journal of Theoretical Biology. 2011;272: 141–144. doi:10.1016/j.jtbi.2010.12.015
10. Altland A, Fischer A, Krug J, Szendro IG. Rare Events in Population Genetics: Stochastic Tunneling in a Two-Locus Model with Recombination. Phys Rev Lett. 2011;106: 88101. doi:10.1103/PhysRevLett.106.088101
11. Jain K. Time to fixation in the presence of recombination. Theoretical Population Biology. 2010;77: 23–31. doi:10.1016/j.tpb.2009.10.005
12. Weinreich DM, Chao L, Phillips P. Rapid evolutionary escape by large populations from local fitness peaks is likely in nature. Evolution. 2005;59: 1175–1182. doi:10.1554/04-392
13. Kondrashov FA, Kondrashov AS. Multidimensional epistasis and the disadvantage of sex. PNAS. 2001;98: 12089–12092. doi:10.1073/pnas.211214298
14. Watson RA, Weinreich DM, Wakeley J. Genome Structure and the Benefit of Sex. Evolution. 2011;65: 523–536. doi:10.1111/j.1558-5646.2010.01144.x
15. de Visser JAGM, Park S-C, Krug J. Exploring the effect of sex on empirical fitness landscapes. Am Nat. 2009;174 Suppl 1: S15-30. doi:10.1086/599081
16. Moradigaravand D, Engelstädter J. The Effect of Bacterial Recombination on Adaptation on Fitness Landscapes with Limited Peak Accessibility. PLoS Comput Biol. 2012;8: e1002735. doi:10.1371/journal.pcbi.1002735
17. Nowak S, Neidhart J, Szendro IG, Krug J. Multidimensional Epistasis and the Transitory Advantage of Sex. PLOS Comput Biol. 2014;10: e1003836. doi:10.1371/journal.pcbi.1003836
18. Moradigaravand D, Kouyos R, Hinkley T, Haddad M, Petropoulos CJ, Engelstädter J, et al. Recombination Accelerates Adaptation on a Large-Scale Empirical Fitness Landscape in HIV-1. PLOS Genet. 2014;10: e1004439. doi:10.1371/journal.pgen.1004439
19. Crona K. Recombination and peak jumping. arXiv:14112017 [q-bio]. 2014; Available: http://arxiv.org/abs/1411.2017

20. Cooper JD, Neuhauser C, Dean AM, Kerr B. Tipping the mutation–selection balance: Limited migration increases the frequency of deleterious mutants. Journal of Theoretical Biology. 2015;380: 123–133. doi:10.1016/j.jtbi.2015.05.003
21. Martens EA, Hallatschek O. Interfering Waves of Adaptation Promote Spatial Mixing. Genetics. 2011;189: 1045–1060. doi:10.1534/genetics.111.130112
22. Crow JF, Kimura M. Evolution in Sexual and Asexual Populations. The American Naturalist. 1965;99: 439–450.
23. Manly BFJ. Randomization, Bootstrap and Monte Carlo Methods in Biology, Third Edition. CRC Press; 2006.
24. Watson RA, Jansen T. A Building-block Royal Road Where Crossover is Provably Essential. Proceedings of the 9th Annual Conference on Genetic and Evolutionary Computation. New York, NY, USA: ACM; 2007. pp. 1452–1459. doi:10.1145/1276958.1277224
25. Szendro IG, Schenk MF, Franke J, Krug J, Visser JAGM de. Quantitative analyses of empirical fitness landscapes. J Stat Mech. 2013;2013: P01005. doi:10.1088/1742-5468/2013/01/P01005

Supplemental Figures

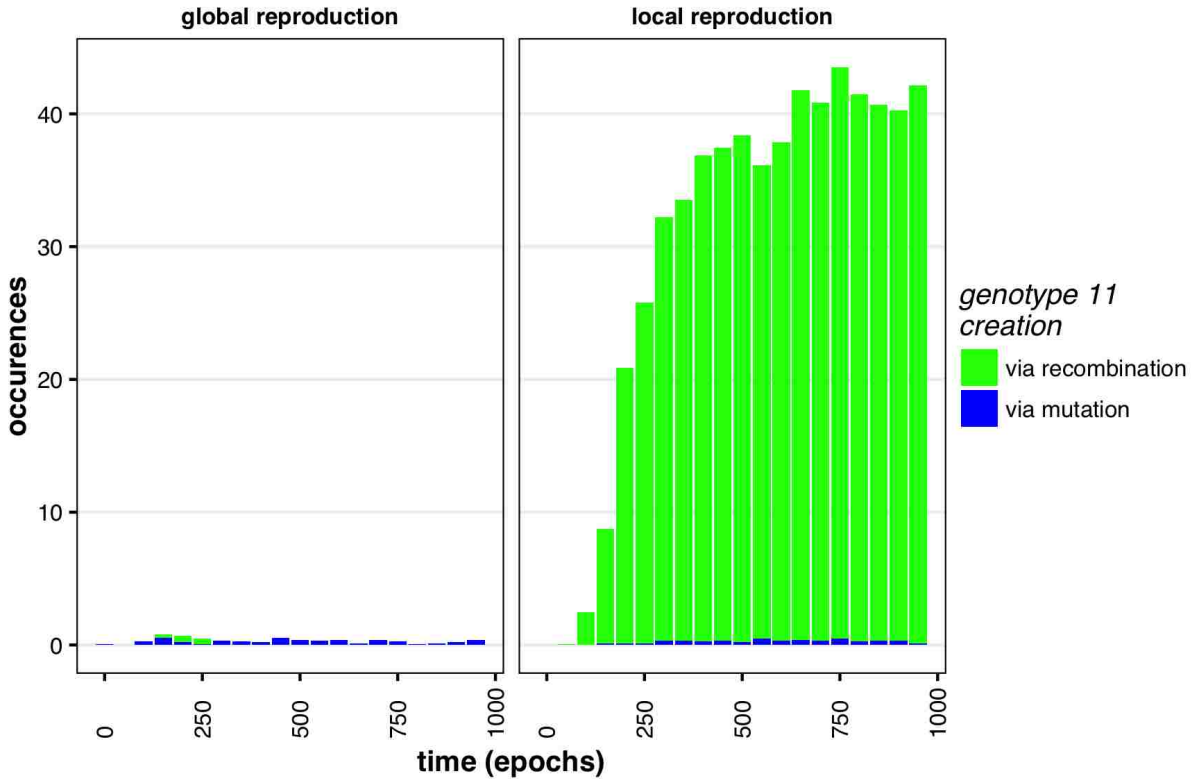

Supplemental Figure 1. "Sutures" between suboptimal peaks allow landscape exploration. Populations are initialized with genotype 00 on a fitness landscape with peak genotypes 01 and 10. Lethal genotype 11 is created via recombination (green bars) frequently only when reproduction is local. Genotype 11 is created via mutation (blue bars) at a low rate at both reproductive distances. Bars represent mean values of 15 replicate simulations using parameter values $L = 70$, $\mu = 10^{-5}$, $f_{11} = 0$, $s_{00} = 0.6$, $s_{10} = s_{01} = 0.85$, $s_{11} = 0$.

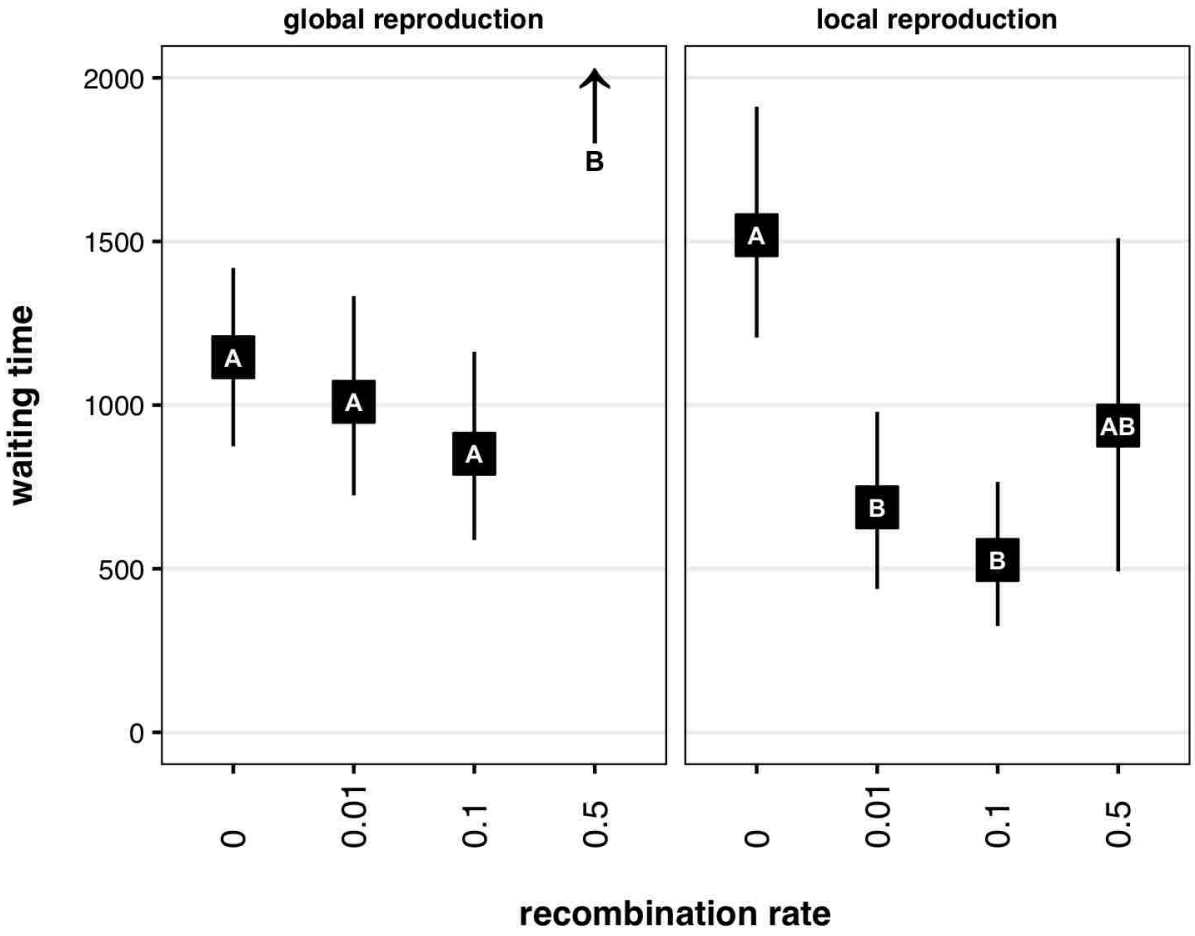

Supplemental Figure 2. Similar to Figure 1, but with organisms of six loci (rather than four), and six suboptimal peaks (rather than two). The pattern seen in Figure 1 appears more pronounced, likely due to increased opportunity for peak-jumping. Data points and error bars represent mean values and standard error of 25 replicate simulations using parameter values $L = 70$, $\mu = 0.002$, $s_G = 0.2$, $s_{000000} = 0.6$, $s_{110000} = s_{001100} = s_{000011} = 0.85$, $s_{111100} = s_{110011} = s_{001111} = 0.9$, $s_{111111} = 0.95$, where G represents all non-specified genotypes. Data points with no shared letter are significantly different (Tukey's HSD, $\alpha = 0.05$). The upward arrow indicates that establishment never occurred by the simulation maximum of 20,000 epochs.

[Supplemental Video]

Supplemental Video. Population composition through time of the simulations depicted in Figure 2. The starting genotype (0000) is represented by green; the two other suboptimal peak genotypes (0011 and 1100) are represented by red and purple, respectively; the optimal genotype (1111) is represented by yellow. All other genotypes are represented by grey.

Appendix

De Visser et al (2009) created their empirical fitness landscapes (which they call CS1 and CS2) by measuring growth rates of all 32 relevant genotypes, and define relative fitness as a genotype's growth rate divided by the maximum growth rate of that landscape's genotypes. We convert these fitnesses (ω_G) to survival probabilities (s_G) with the formula $s_G = \frac{\omega_G}{2\overline{\omega}}$, where $\overline{\omega}$ is the average fitness on the landscape.

	PJ^+ (CS1)		PJ^- (CS2)	
genotype	ω_G	δ_G	ω_G	δ_G
00000	1.000	0.638	1.000	0.628
10000	0.878	0.560	0.878	0.551
01000	0.835	0.533	0.835	0.524
00100	0.870	0.555	0.870	0.546
00010	0.772	0.493	0.909	0.571
00001	0.793	0.506	0.772	0.485
11000	0.865	0.552	0.865	0.543
10100	0.854	0.545	0.854	0.536
10010	0.773	0.493	0.923	0.580
10001	0.873	0.557	0.773	0.485
01100	0.816	0.521	0.816	0.512
01010	0.716	0.457	0.852	0.535
01001	0.848	0.541	0.716	0.450
00110	0.778	0.497	0.855	0.537
00101	0.820	0.523	0.778	0.488
00011	0.972	0.620	0.785	0.493
11100	0.816	0.521	0.816	0.512
11010	0.748	0.477	0.879	0.552
11001	0.832	0.531	0.748	0.470
10110	0.749	0.478	0.942	0.592
10101	0.792	0.506	0.749	0.470
10011	0.753	0.481	0.795	0.499
01110	0.617	0.394	0.858	0.539
01101	0.810	0.517	0.617	0.387
01011	0.643	0.410	0.724	0.455
00111	0.671	0.428	0.745	0.468
11110	0.690	0.440	0.825	0.518
11101	0.855	0.546	0.690	0.433
11011	0.649	0.414	0.665	0.418
10111	0.692	0.442	0.686	0.431
01111	0.643	0.410	0.640	0.402
11111	0.645	0.412	0.622	0.391
mean	**0.783**	**0.500**	**0.796**	**0.500**
SD	**0.095**	**0.061**	**0.095**	**0.060**

1344

1345

1346

Chapter 3

David slays Goliath 'discretely':
Competitive reversals through oscillations and chaos

Jacob D Cooper[1], Clarence Lehman[2], Richard McGehee[3], and Benjamin Kerr[1]

[1] *Department of Biology, University of Washington, Seattle, WA*
[2] *Department of Ecology, Evolution, and Behavior, University of Minnesota, Minneapolis, MN*
[3] *School of Mathematics, University of Minnesota, Minneapolis, MN*

Running title:
David slays Goliath 'discretely'

Corresponding author:
Benjamin Kerr
University of Washington
Department of Biology
Box 351800
Seattle, WA 98195-1800
phone: (206) 221-7026
email: kerrb@uw.edu

Keywords:
discrete population dynamics
Ricker model
coexistence
Hassell model
Lotka-Volterra

Abstract:

Many species reproduce in discrete bursts, often synchronized with the seasons. Although such discrete-time dynamics of single populations have been modeled systematically, the corresponding theory for multiple populations is less developed. Here we show that classical rules for predicting competitive outcomes are appropriate for a certain subset of discrete-time systems, which motivates a new discrete-time competitive exclusion principle. Nonetheless, classical rules can fail dramatically for other discrete-time systems. As a striking example, a classically inferior species (e.g., low K or high R*) can drive a classically superior competitor (high K or low R*) to extinction. The reasons relate to (1) the shifting of statistical moments in abundance accompanying population fluctuations (cycles or chaos), and (2) how such moments are filtered by non-linearities in the logarithm of growth curves. We discuss some implications of these results for competition theory as well as other applications, including management and epidemiology.

Introduction

The introduction of discrete-time population dynamics into ecology was a theoretical bombshell (Hassell, 1975; Hassell and Comins, 1976; Hassell et al., 1976; May, 1974, 1975; May and Oster, 1976). These early studies demonstrated that population dynamics resulting from structurally simple equations could be richly complex—exhibiting fixed points, cycles, and chaos. Indeed, erratic fluctuations in population data no longer required explanations of experimental error or stochastic noise, but rather could result from completely deterministic density-dependent population growth. There was also something of a heterodox character to these dynamics; discrete-time systems did not behave like their continuous-time counterparts. In this paper, we explore how discrete-time dynamics conform and deviate from expectations from continuous-time theory in the context of multiple competing species.

One of the simplest continuous-time models of ecological communities is the Lotka-Volterra framework for two-species competition. At any instant, the abundances of the two species are given by a point in a phase plane (Fig. 1). Movement of this point represents change in the competitors' abundances. The full dynamics can be discerned from the manner in which the zero-growth curves (isoclines) of the species are positioned. For example, in Figure 1a, the region in which species 1 increases in abundance (dotted red region) completely encloses the corresponding region for species 2 (solid blue region). There are no population values where species 1 decreases while species 2 increases (Figure 1b), and species 1 drives species 2 extinct (Figure 1c). This is a simple example of a more general exclusion principle proved by Volterra (1928) and explored empirically and philosophically by subsequent authors (*e.g.*, Gause, 1934; Hardin, 1960).

1461

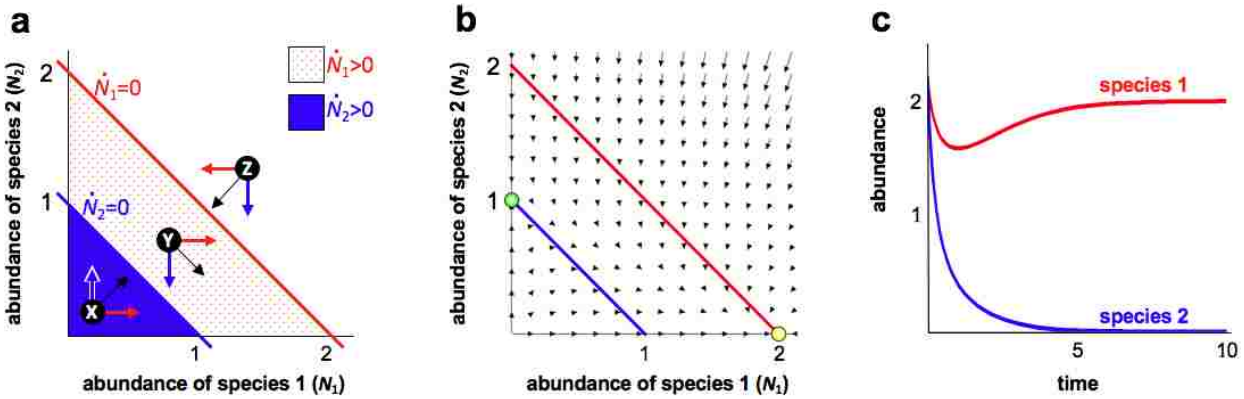

1462 **Figure 1:** Continuous-time competitor dynamics. (a) The dynamics of two competitors are given by
1463 $dN_1/dt=(1-(N_1+N_2)/2)N_1$ and $dN_2/dt=(1-N_1-N_2)N_2$. The isoclines of species 1 and species 2 are red and
1464 blue, respectively. A point in the plane gives species' densities. For three example points (X, Y, and Z),
1465 community change is given (roughly) by the black vector, which is broken into red (change in N_1) and
1466 blue (change in N_2) components. The red-hatched and solid-blue regions indicate where N_1 and N_2
1467 increase, respectively. (b) The corresponding slope field, showing locally stable (yellow circle) and
1468 unstable (green circle) equilibria. (c) The community trajectory when $N_1(0)=N_2(0)=2.2$.
1469

1470 Here we ask how such continuous-time theory translates to discrete-time. Does a species whose region
1471 of increase completely encloses its competitor's (as in Fig. 1a) always have the competitive advantage?
1472 In fact, it is already known that two species can coexist under such circumstances (Adler, 1990;
1473 Asmussen, 1979; Edmunds et al., 2003; Franke and Yakubu, 1991; Gatto, 1993). But, as we outline
1474 below, a stranger turn of events is possible—a traditionally inferior species 2 can increase to high
1475 abundance while driving species 1 extinct, even though at no instant of time does species 2 increase
1476 while species 1 is decreasing. We turn to an example of such a scenario first.

1477

1478 **A Motivating Example**

1479 A generic discrete-time competition model for two species can be expressed as:

1480 $$N_1(t+1) = G_1\big(N_1(t), N_2(t)\big)\, N_1(t) \qquad (1a)$$

1481 $$N_2(t+1) = G_2\big(N_1(t), N_2(t)\big)\, N_2(t) \qquad (1b)$$

where G_i is the factor by which the abundance of species i, N_i, increases (G_i>1) or decreases (G_i<1) from generation t to t+1. Since the species interact, G_i is a function of both species' abundances. Henceforth we assume that growth always slows with increasing abundances ($G_i \to 0$ as $N_1 \to \infty$ or $N_2 \to \infty$) and both species thrive when abundances are low (G_i>1 when $N_1 \approx 0$ and $N_2 \approx 0$).

As a concrete example, consider an extended version of the widely-used Ricker model (Gatto, 1993; May, 1974; Ricker, 1954). In this model,

$$G_i\big(N_1(t), N_2(t)\big) = \exp\Big\{\ln(r_i)\Big(1 - \Big[\big(N_1(t) + N_2(t)\big)/K_i\Big]^{\gamma_i}\Big)\Big\}$$

where r_i is the growth factor when abundances are low, K_i is the carrying capacity, and γ_i is a 'shape parameter' for species i. This model is a discrete-time incarnation of the theta-logistic (Nelder, 1961). In Figure 2, the region of positive growth for species 1 completely encloses that of species 2. We might expect species 1 to out-compete species 2, which is what the isocline arrangement would dictate if reproduction were continuous (*e.g.*, Fig. 1). In fact, species 2 invades from low abundance and coexists with species 1 (Figs. 2a,c). Species 1 likewise invades and coexists (Figs. 2b,d). At higher growth rates of species 2, though the isoclines are unchanged, species 2 invades and displaces species 1 (Figs. 2e,g). The classically superior species 1 cannot invade species 2 (Fig. 2f). It seems we have a competitive David slaying Goliath. What is going on?

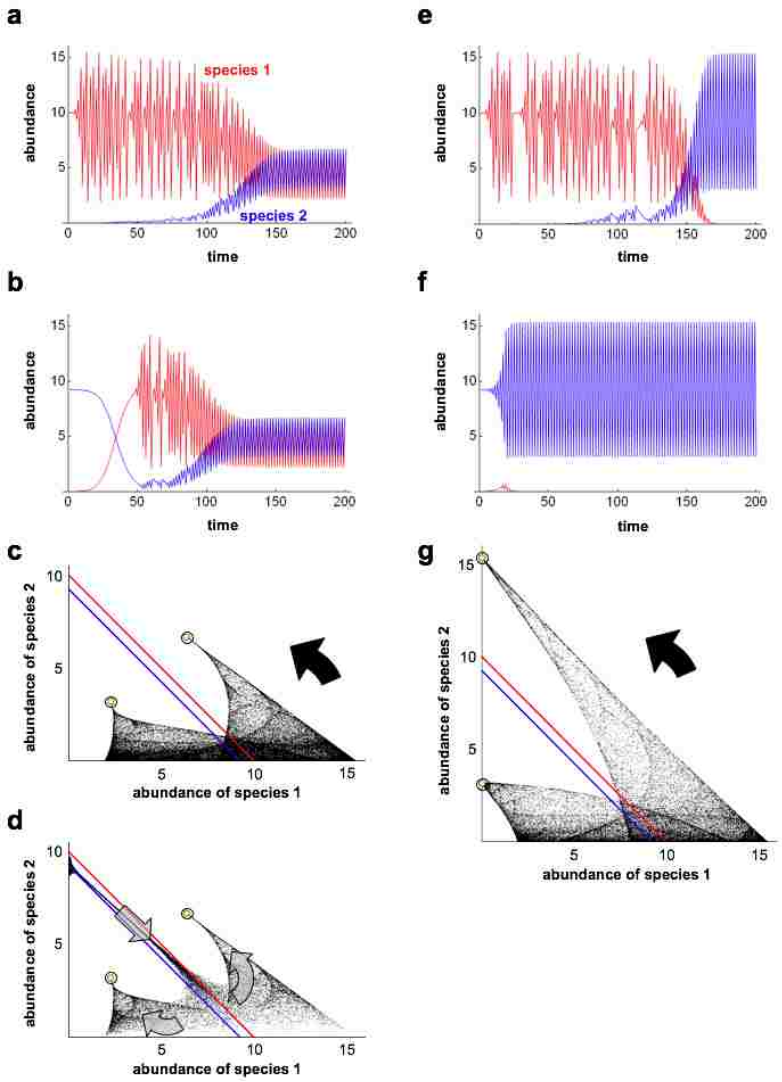

Figure 2: Discrete-time competitor dynamics. (a) Dynamics of two competitors with $G_i=\exp\{\ln(r_i)(1-[(N_1(t)+N_2(t))/K_i]^{\gamma_i})\}$, where $r_1=4.4$, $r_2=6$, $K_1=10$, $K_2=9.25$, $\gamma_1=2$, and $\gamma_2=1$. The isoclines do not cross and species 1 is the classically superior competitor. Nonetheless, species 2 invades and coexists with species 1. (b) Coexistence also results when species 1 starts rare and species 2 begins near its fixed point. (c) A phase plane representation of the dynamics from part a. We ran 500 simulations with different initial conditions where a small point giving abundances was plotted for 1000 time steps each. The community starts near species 1's axis and proceeds (curved black arrow) through oscillations of decreasing complexity to a period-2 cycle with both species coexisting (yellow circles with rings). The isoclines are also shown. (d) A phase plane representation of the dynamics from part b (500 simulations). The community moves off species 2's axis toward extinction of species 1 (straight grey arrow) until oscillations develop and the community turns around (curved grey arrows), approaching the same period-2 cycle. (e) The model from part a, except with $r_2=11$. Species 2 now *replaces* species 1 when starting from a low abundance. (f) Species 2 resists invasion by species 1. (g) A phase plane representation (500 simulations) of the dynamics from part e. The chaotic trajectory on the N_1 axis is unstable to invasion by species 2 (curved black arrow), whereas the period-2 cycle on the N_2 axis is stable to invasion by species 1 (yellow circles with rings).

Oscillations are a conspicuous feature in Figure 2. Coexistence of multiple species on fewer resources than predicted by classical theory has been shown to occur when populations oscillate periodically or chaotically, in both continuous-time (Armstrong and McGehee, 1980; Huisman and Weissing, 1999; Vandermeer et al., 2002) and discrete-time (Adler, 1990; Asmussen, 1979; Edmunds et al., 2003; Franke and Yakubu, 1991; Gatto, 1993). When systems are oscillating, conclusions based on equilibria (or isoclines) can be unreliable. Is it ever reasonable to expect information about where abundance is static (*e.g.*, equilibria) to say something useful about systems where abundance is perpetually changing? Interestingly, the answer is 'yes.' For a class of common discrete-time systems, equilibria tell the *whole* story about competitive outcomes, even when the system oscillates wildly and never reaches equilibrium. For such systems we present and prove a competitive exclusion principle, which corresponds to expectations from continuous-time theory (Volterra, 1928). We then show how models outside of this class (*e.g.*, Fig. 2) can overturn our expectations.

Discrete-Time Competitive Exclusion Principle

Consider a community of S competitors in which the dynamics of species i is:

$$N_i(t+1) = G_i\big(\mathbf{N}(t)\big)N_i(t) \qquad (2)$$

where $\mathbf{N}(t) \equiv \langle N_1(t), N_2(t), N_3(t), \dots, N_S(t)\rangle$ gives the abundances of each species at t. Equation (2) generalizes equation (1). Let $\mathbf{N}_i(t) \equiv \langle 0, 0, 0, \dots, 0, N_i(t), 0, \dots, 0\rangle$, where only species i is present (at density $\mathbf{N}_i(t)$); and $\vec{\mathbf{0}} \equiv \langle 0, 0, 0, \dots, 0\rangle$, where all species are absent.

Here we describe competition for a type of common "abiotic resource" (*sensu* Armstrong and McGehee, 1980). We will call a community "Volterrian" if the logarithm of each growth factor can be written as follows:

$$\ln G_i\big(\mathbf{N}(t)\big) = \alpha_i - \beta_i\, H\big(\mathbf{N}(t)\big) \tag{3}$$

where $i \in \{1, 2, 3, \ldots, \mathrm{S}\}$, and with $\alpha_i > 0$ and $\beta_i > 0$. H is a continuous function with $H\big(\vec{\mathbf{0}}\big) = 0$, $\partial H/\partial N_i > 0$, and $\lim_{N_j \to \infty} H(\mathbf{N}) = \infty$, for all $j \in \{1, 2, 3, \ldots, \mathrm{S}\}$ and any $\mathbf{N}$. Finally, we require that $H(\mathbf{N}_i)=H(\mathbf{N}_j)$ whenever $\|\mathbf{N}_i\| = \|\mathbf{N}_j\|$ (we note that the norm $\|\mathbf{N}_i(t)\| = N_i(t)$ here). The function H gauges the negative impact of species on the shared "abiotic resource." Condition (3) describes a class of models that includes familiar members (Table 1).

Table 1: **Models obeying the competitive exclusion principle**

Model*	Growth Factor (G_i)	Single-Species Equilibrium ($\widehat{\boldsymbol{N_i}}$)	Condition (3) Details†		
			α_i	β_i	$H(x)$
Ricker‡	$\boldsymbol{\exp\left\{\ln r_i\left[1 - \left(\frac{\sum_{j=1}^{S} N_j(t)}{K_i}\right)^{\gamma}\right]\right\}}$	$\boldsymbol{K_i}$	$\boldsymbol{\ln r_i}$	$\boldsymbol{\frac{\ln r_i}{K_i}}$	$\boldsymbol{x^{\gamma}}$
Hassell§	$\boldsymbol{\frac{\lambda_i}{\left(1 + a\sum_{j=1}^{S} N_j(t)\right)^{b_i}}}$	$\boldsymbol{\frac{\exp(\lambda_i/b_i) - 1}{a}}$	$\boldsymbol{\ln \lambda_i}$	$\boldsymbol{b_i}$	$\boldsymbol{\ln(1 + ax)}$
Unnamed	$\boldsymbol{\lambda_i\left\{\exp\left(1 - \exp\left(\sum_{j=1}^{S} N_j(t)\right)\right)\right\}^{w_i}}$	$\boldsymbol{\ln(\ln v_i/w_i + 1)}$	$\boldsymbol{\ln v_i}$	$\boldsymbol{w_i}$	$\boldsymbol{\exp(x) - 1}$

† In all cases shown the variable x is total abundance: $x = \sum_{j=1}^{S} N_j(t)$
* In all of the models presented, standard competition coefficients are assumed to be unity
‡ This is an extended version of the standard Ricker model (as normally γ=1).
§ In this version of the Hassell model, the parameter a is assumed to be the same for every competitor.

In a Volterrian community, if species k has the highest equilibrium abundance when alone, it will displace all other species. We prove this in Appendix A and show how a community can be isolated to a shifting lower-dimensional subspace during its trajectory. Thus, condition (3) yields a competitive

exclusion principle, which operates regardless of oscillations (Supplementary Information, section B.7). Even if trajectories are chaotic, in Volterrian communities, there is order in the chaos.

In Figure 3, the equilibrium abundance of species 1 is slightly greater than species 2 for two communities satisfying condition (3). Despite oscillations, species 1 displaces species 2, dynamically etching a bifurcation diagram in the phase plane. This outcome is in agreement with the classical expectations based on isocline or other analyses.

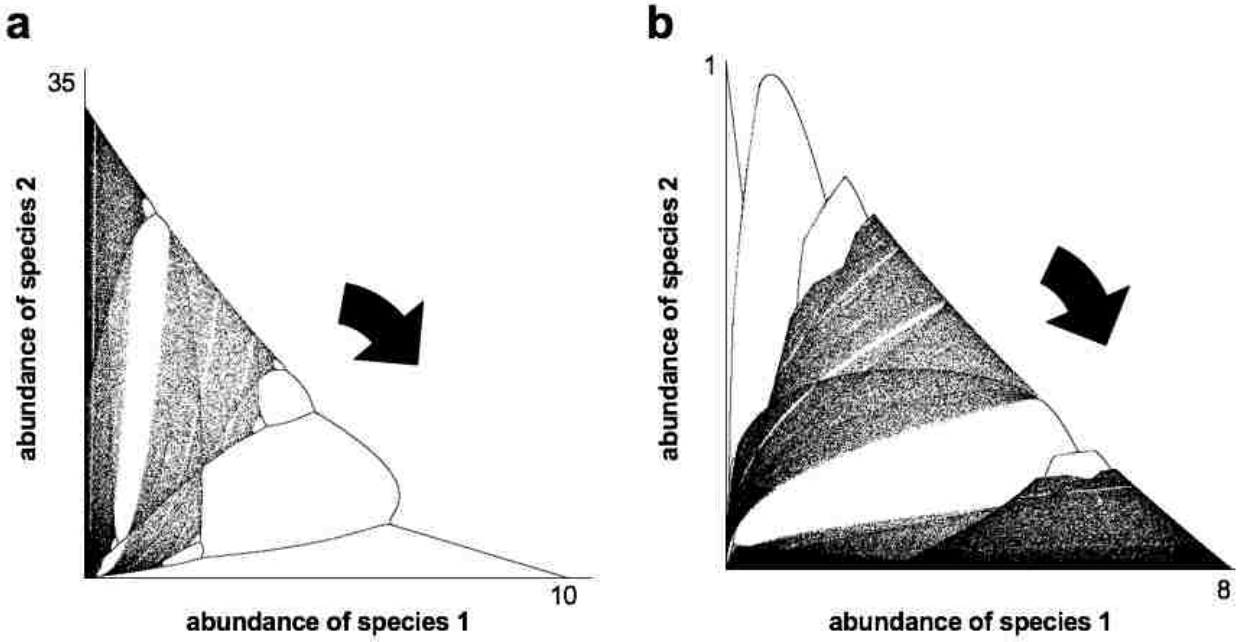

Figure 3: Illustrations of the competitive exclusion principle. (a) The Ricker model (Table 1) with r_1=3, r_2=30, K_1=10, K_2=9.995, γ=1. A phase plane representation in which species 1 starts out rare and species 2 starts out common. We ran 10 simulations (80,000 time steps each) with slightly different initial conditions, plotting a small point for abundances at each time step. The community starts near species 2's axis and proceeds (curved black arrow) through oscillations of decreasing complexity to a fixed point with species 1 excluding species 2. (b) The Hassell model (Table 1) with λ_1=150, λ_2=8, b_1=7.2284, b_2=3, a=1. The community starts near species 2's axis and proceeds (curved black arrow) through oscillations of increasing complexity to a chaotic trajectory with species 1 excluding species 2.

Explaining Unexpected Outcomes

Communities that do not satisfy condition (3) can violate classical expectations. Consider a two-species community where species 1 is a resident and species 2 is a rare invader. When extremely rare, the appropriate measure for the invader's long-term growth is $\widetilde{G_2} = \lim_{T\to\infty} \sqrt[T]{\prod_{t=0}^{T-1} G_2(N_1(t),0)}$. Mathematically, $\widetilde{G_2}$ is a Lyapunov number (Ferriere and Gatto, 1995; Gatto, 1993; Hastings et al., 1993; Metz et al., 1992). For species 2 to increase from rarity, $\widetilde{G_2}$ must exceed 1. Using an approach similar to Chesson's (2000), this growth rate can be approximated as:

$$\widetilde{G_2} \approx G_2(\overline{N}_1, 0) e^{(\delta_2/2)\sigma^2_{N_1}}, \tag{4a}$$

where

$$\delta_2 = \frac{d^2 \ln G_2(n,0)}{dn^2}\Big|_{n=\overline{N_1}} \tag{4b}$$

Equations (4) define an 'invasion heuristic' (Appendix B outlines the derivation for two species and the heuristic is generalized in the Supplementary Information, section C). Because our invasion heuristic highlights measurable quantities, such as the mean ($\overline{N_1}$) and variance ($\sigma^2_{N_1}$) in resident abundance, it is an empirically useful approximation of the Lyapunov number (see Ferriere & Gatto (1995) for details on Lyapunov analysis). The heuristic is generally suitable when the fluctuations in the resident's abundance are small.

A smaller mean abundance in a fluctuating resident, $\overline{N_1}$, will make $G_2(\overline{N_1}, 0)$ greater, which helps the invader. The effect of the variance in resident abundance, $\sigma^2_{N_1}$, depends on the sign of δ_2, which reflects the curvature of the invader's growth function. If $\ln G_2$ is concave (δ_2<0), then a lower variance in the resident's abundance will make $e^{(\delta_2/2)\sigma^2_{N_1}}$ larger, helping the rare species invade. On the other hand, if $\ln G_2$ is convex (δ_2>0), a higher resident variance helps the rare species.

1598 Thus, in the first approximation, successful invasion depends on the shape of the invader's growth
1599 function and on the statistical moments of the resident's population distribution. Such moments change
1600 with parameter values like the resident's intrinsic growth rate, r_1. The bifurcation diagrams in Figure 4
1601 show how the variance of the resident tends to increase with r_1. If the resident oscillates, its mean
1602 abundance is affected by the shape of its own growth curve. If the logarithm of the resident's growth
1603 function is concave, then the mean abundance of a fluctuating population is less than its single-species
1604 equilibrium. However, if the fluctuating resident's growth function is log-convex, then mean
1605 abundance is greater than its single-species equilibrium (Supplementary Information, section A.4). In
1606 general, if the resident's growth function is log-concave, larger oscillations will lower average
1607 abundance; whereas if the growth function is log-convex, oscillations will raise average abundance
1608 (Figs. 4a and 4c).
1609
1610
1611

1612

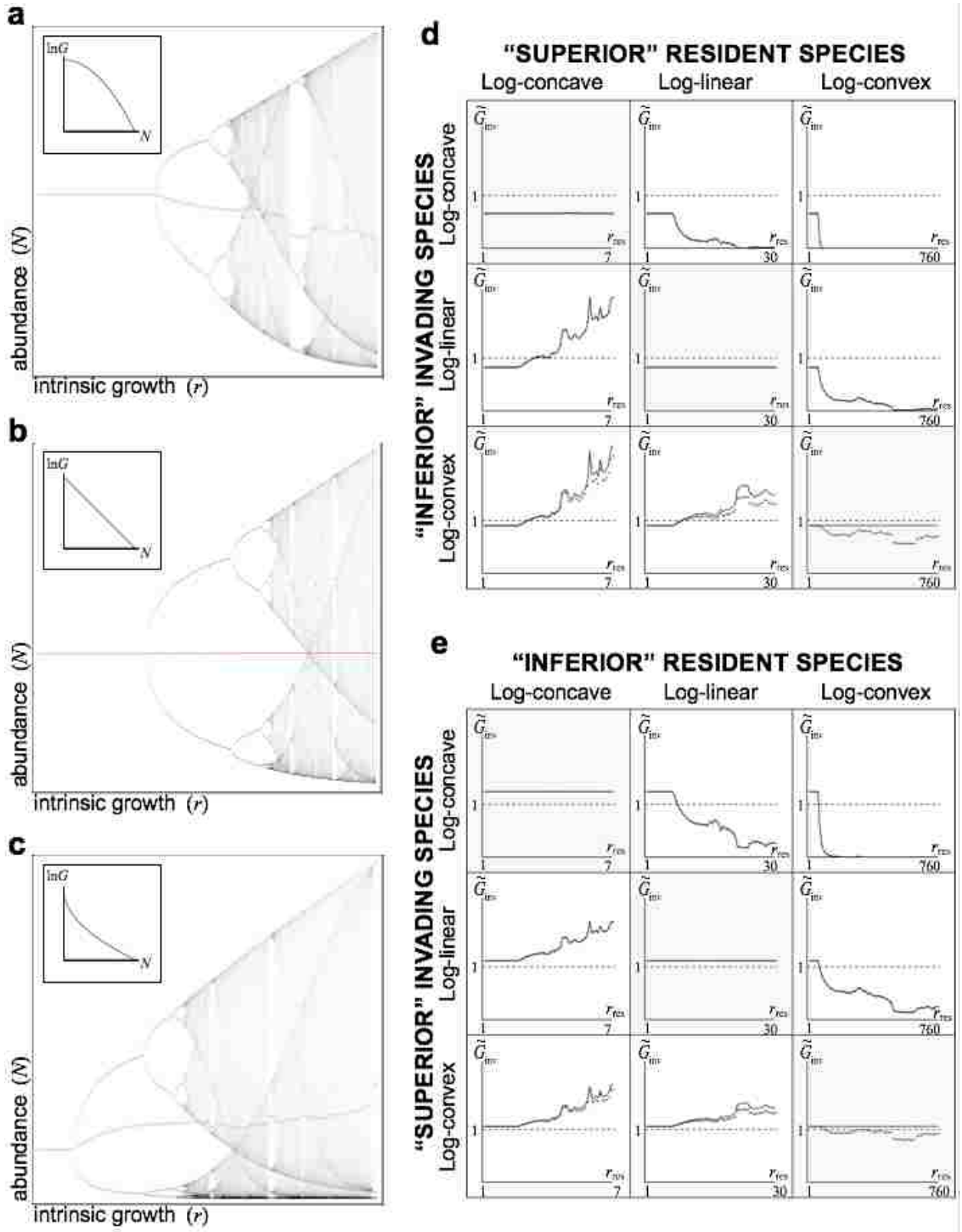
a
b
c
lnG
N
abundance (N)
intrinsic growth (r)
d
"SUPERIOR" RESIDENT SPECIES
Log-concave
Log-linear
Log-convex
"INFERIOR" INVADING SPECIES
e
"INFERIOR" RESIDENT SPECIES
"SUPERIOR" INVADING SPECIES

Figure 4: Effects of growth function log-concavity. (a) For a single-species Ricker model (Table 1), if $\gamma>1$, $\ln G$ is concave (inlet: $\gamma=2$). The bifurcation diagram gives long-term abundances as a function of intrinsic growth rate (more intensely visited regions are darker grey). The mean abundance (red line) decreases below the carrying capacity as fluctuations develop. (b) When $\gamma=1$, $\ln G$ is linear. The mean abundance does not deviate from the carrying capacity as fluctuations develop. (c) When $\gamma<1$, $\ln G$ is convex (inlet: $\gamma=½$). As fluctuations develop, the mean abundance increases above the carrying capacity. (d) A two-species model with $G_i=\exp\{\ln(r_i)(1-[(N_1(t)+N_2(t))/K_i]^{\gamma_i})\}$ and $r_{inv}=11$, $K_{res}=10$, $K_{inv}=9.25$. We use $\gamma_i=2$, $\gamma_i=1$, and $\gamma_i=0.5$ for log-concave, log-linear, and log-convex growth, respectively. From classical analysis, the resident is "superior." We plot the invader's long-term growth ($\widetilde{G}_{inv}$) in terms of the resident's intrinsic growth rate (r_{res}) for different log-concavity combinations. The dots are from (4), using simulated resident moments. The jagged line is the invader's growth computed as the long-term geometric mean. For $\gamma_{inv}=1$ or $\gamma_{inv}=2$, approximation (4) is exact. When $\gamma_{inv}=\gamma_{res}$ our exclusion principle applies (row 1, Table 1). However, when the "inferior" invader has a growth function that is more log-convex than the "superior" resident, then the invader's long-term growth factor can be greater than unity (i.e., it can invade). This can be due to a "mean effect": the oscillation-mediated reduction in the resident's mean abundance (2nd row, 1st column); a "variance effect": the oscillation-mediated increase in the invader's effective growth (3rd row, 2nd column); or both (3rd row, 1st column). (e) The same model as in part d, except $r_{inv}=4.4$, $K_{res}=9.25$, $K_{inv}=10$. Now the invader is "superior." Approximation (4) can be inaccurate, as seen when both species have log-convex growth. The "superior" competitor may not be able to invade (long-term growth drops below unity) due to a "mean effect", a "variance effect" or both (plots above the diagonal). Figure 2 can be understood by making species 1 the "superior" and species 2 the "inferior" and looking at the plot in 2nd row and 1st column of part d and the plot in the 1st row and 2nd column of part e.

Now it can be seen why a traditionally inferior competitor need not be inferior under discrete reproduction. When species 1 in Figure 2 is alone with a low growth rate (r_1), its abundance is equal to its carrying capacity (K_1). However, at higher growth rates, species 1 can oscillate. For the parameters in Figures 2a-d, species 1 follows a chaotic trajectory if alone. Because the growth function of species 1 is log-concave, oscillations lower its mean abundance below K_1. Consequently, as an invader, species 2 'feels' a lower abundance of its competitor, on average, than it would if species 1 were at its fixed point. Given that the growth curve of species 2 is log-linear, the invading species 2 is aided by species 1's changed mean (lower $\overline{N_1}$ increases $\widetilde{G_2}$) while it is unaffected by species 1's changed variance (higher $\sigma^2_{N_1}$ does not change $\widetilde{G_2}$ when $\delta_2=0$).

The same analysis is relevant when considering species 2 as the resident and species 1 as the invader (*i.e.*, $\widetilde{G_1} \approx G_1(0, \overline{N_2}) e^{(\delta_1/2)\sigma^2_{N_2}}$ with $\delta_2 = \{d^2 \ln G_2(n,0)/dn^2\}|_{n=\overline{N_1}}$). Consider the case of coexistence (Figs. 2a-d). Here, species 2 approaches its carrying capacity when alone (r_2 small—see Fig. 4b). In such a case, $\sigma^2_{N_2} = 0$, $\overline{N_2} = K_2$, and $G_1(0, K_2) > 1$. Consequently, $\widetilde{G_1} > 1$ and species 1 can invade. Thus, for Figures 2a-d, $\widetilde{G_1} > 1$ and $\widetilde{G_2} > 1$. In this case, coexistence results.

However, what happens if the intrinsic growth of species 2 increases, such that it oscillates when alone? In such a case, $\sigma^2_{N_2} > 0$ and $\overline{N_2} = K_2$ (due to log-linear growth). Given that species 1's growth is log-concave, the variance in species 2 harms the invasion potential of species 1 ($\widetilde{G_1}$ decreases as $\sigma^2_{N_2}$ increases when $\delta_1<0$). It is possible for $\widetilde{G_1} < 1$ if the variance in species 2 is large enough. The end result is that species 2 replaces species 1 (Figs. 2e-g)—opposite of expectations from continuous-time theory and our exclusion principle (compare the axis bearing yellow circles in Fig. 2g to that in Fig. 1b). Such reversals can also occur in the simplest resource-based competition models. R^* is a measurable resource level below which a given species grown in monoculture cannot persist (Tilman, 1982). Classically, the species with the lowest R^* displaces its competitors. Yet when reproduction occurs discretely, a species with a higher R^* can displace one with a lower R^* (Supplementary Information, section D.3).

In the case of Figure 2, condition (3) is violated because $\gamma_1 \neq \gamma_2$. When $\gamma_1 = \gamma_2 = \gamma$, condition (3) is satisfied (Table 1) and classical expectations hold (Fig. 3a). The parameter γ_i controls the log-concavity of the growth function of species i. By setting γ_1=2 and γ_2=1, the log-concavities of the two species differ (a form of relative non-linearity (Chesson, 2000)). As a resident, species 1 is harmed by its own fluctuations. As an invader, species 1 is harmed by the fluctuations in species 2. Meanwhile, species 2

1670 is not directly affected by fluctuations in the system. Thus, as the community experiences larger
1671 fluctuations (as r_1 and r_2 increase), the outlook for species 2 can improve to the point of exclusion of
1672 the classically superior species 1. Given differences in log-concavity, changes to the mean resident
1673 abundance ($\overline{N_i}$), variance in resident abundance ($\sigma^2_{N_i}$), or both simultaneously can lead to a reversal of
1674 fortune for an invader (Figs. 4d,e). Growth log-concavities are critical because the shape of the growth
1675 curve affects the mean abundance of a resident as well as the way that an invader 'filters' the variance
1676 in a resident.
1677
1678 **Discussion**
1679 The ecological theory of interacting species has developed over almost a century and has illuminated a
1680 diversity of applications, including management of wildlife populations, harvesting of natural
1681 resources, and control of epidemics. Much of this theory concerns species that reproduce continuously
1682 throughout the year, yet many species in nature reproduce only at discrete times, often synchronised
1683 with the seasons.
1684
1685 In May's classic paper, he outlined how simple density dependent growth in a single species in a
1686 discrete-time framework could produce dynamics foreign to an equivalent continuous-time framework
1687 (May, 1974). At the end of the very same paper, May discussed deviation between a discrete-time two-
1688 species version of the Lotka-Volterra model and its continuous-time equivalent. The continuous-time
1689 Lotka-Volterra model predicts four basic competitive outcomes depending on the orientation of
1690 isoclines: (i) species 1 excludes species 2, (ii) species 2 excludes species 1, (iii) both species coexist, or
1691 (iv) either species can exclude the other depending on initial conditions (bistability). For discrete
1692 models that do not satisfy condition (3), we have shown that expectations based on this Lotka-Volterra
1693 framework can be misleading. Indeed, all four dynamical outcomes are consistent with a single

1694 isocline arrangement (Supplementary Information, section D.1). Furthermore, novel outcomes are
1695 possible and lead to potential applications in the laboratory and the field.
1696
1697 A first sample application is Park's famous *Tribolium* competition experiments. These have often been
1698 interpreted using the standard Lotka-Volterra taxonomy (see Edmunds *et al*. (2003) for a historical
1699 overview), in spite of the fact that Park discovered unconventional competitive outcomes in a final
1700 experiment with two competitors (Leslie et al., 1968). In most of the competitions, Park observed that
1701 one species excluded the other (consistent with bistability); but, in one competition, the two species
1702 were found to coexist over 30 generations. Discrete time models incorporating life cycle stages (e.g.,
1703 larvae, pupae, and adults) have showcased the existence of multiple attractors corresponding to both
1704 coexistence and exclusion that are consistent with these results (Cushing et al., 2004; Edmunds et al.,
1705 2003). However, it has been posed as an open question (Cushing et al., 2004) whether simple
1706 competition models without explicit life cycle stages (such as the two-species Ricker) can also
1707 demonstrate such dynamics. Figures 5a and 5b address this question by showing that the extended
1708 Ricker is capable of producing such multiple attractors (we show cases with one exclusion attractor
1709 and one coexistence attractor). Due to oscillations and a difference in the log-concavity of growth
1710 between species, traditional cases of bistability (Fig. 5a) and coexistence (Fig. 5b) are transformed into
1711 these novel competitive outcomes.
1712

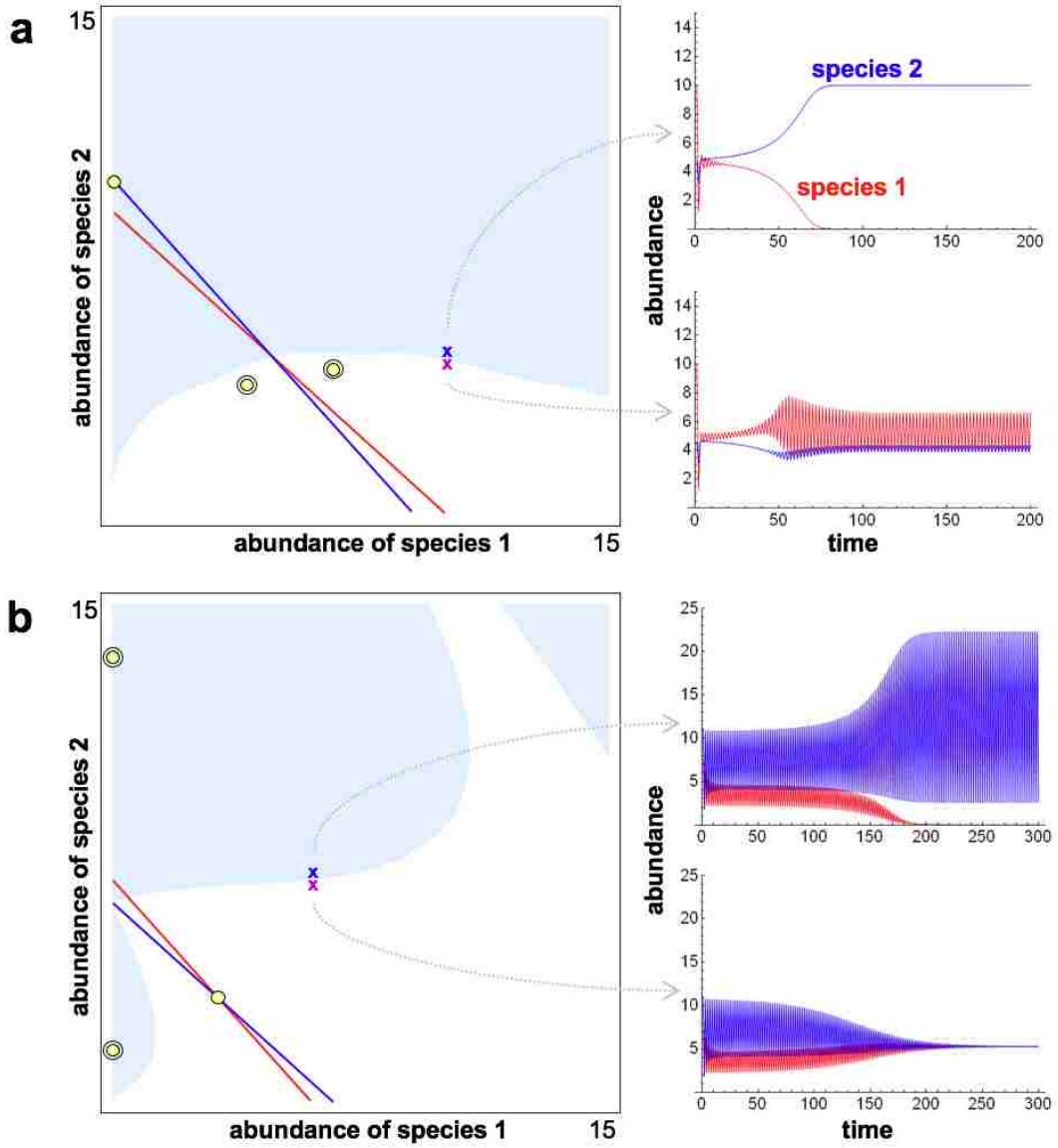

Figure 5: Multiple attractors. (a) Dynamics of two competitors with growth functions given by $G_i=\exp\{\ln(r_i)(1-[(N_i(t)+c_{ij}N_j(t))/K_i]^{\gamma_i})\}$, where $r_1=5$, $r_2=2$, $K_1=K_2=10$, $\gamma_1=2$, $\gamma_2=1$, $c_{12}=c_{21}=1.1$. Note that c_{ij} is the standard "competition coefficient" and that condition (3) may not be satisfied upon inclusion of arbitrary coefficients (previously we have assumed $c_{ij}=c_{ji}=1$). Here the classical expectation from isocline orientation is bistability, where one or the other species, but not both, can persist. Instead we find coexistence (approaching a period-2 cycle) from the initial conditions given in white region and exclusion of species 1 by species 2 from the initial conditions given by the blue region. Example trajectories are shown to the right, corresponding to initial conditions given by the "x's". (b) The same model with $r_1=7$, $r_2=80$, $K_1=K_2=10$, $\gamma_1=0.9$, $\gamma_2=0.5$, $c_{12}=c_{21}=0.9$. Here the classical expectation (from isocline orientation) is coexistence. Instead we find coexistence (approaching a fixed point) from the initial conditions given in white region and exclusion of species 1 by species 2 (approaching a period 2 cycle) from the initial conditions given by the blue region. Example trajectories are shown to the right, corresponding to initial conditions given by the "x's".

A second sample application of our framework involves the management of harvested species. Some species are managed so that harvesting only occurs once an abundance threshold is surpassed (Lande et al., 1997). If the managed species has a competitor and both species reproduce in discrete events, then it is theoretically possible that a management policy of this kind will actually drive the competitor of the managed species extinct. This can occur because the competitor may depend on existing fluctuations in the managed species. If harvesting has the effect of reducing these fluctuations (Lande et al., 1997), the competitor can permanently exit the system (Supplementary Information, Fig D4a). On the flip side, Anderson *et al*. (2008) have suggested that harvesting may *destabilize* populations, perhaps due to selection for altered intrinsic growth rates. In the Supplementary Information, we demonstrate that selection for a higher growth rate in one harvested species can drive a competitor extinct (Fig. D4c). These harvesting impacts can also have the reverse effect, allowing a previously excluded competitor to invade (Supplementary Information, Figs. D4b and D4d).

A third sample application of our framework shows that these same ideas are not restricted to ecological competition alone but apply to other species interactions. In epidemiology, the quantity R_0 is related to the rate of increase of a pathogen when extremely rare. If $R_0<1$, the disease declines to extinction. Generally, R_0 is evaluated at some equilibrium host abundance. However, if the host population (with a log-convex growth curve) reproduces discretely, then a disease can spread even when the equilibrium-based $R_0<1$ (Supplementary Information, Fig. D5a). Conversely, oscillations in a host (with a log-concave growth curve) could force the disease extinct even if the equilibrium-based $R_0>1$ (Supplementary Information, Fig. D5b). Thus, it is essential to consider host fluctuations when predicting the likelihood of an epidemic.

1750 Beyond these sample applications, many species in nature exhibit discrete bursts of reproduction,
1751 frequently coincident with seasonal patterns (*e.g.*, annual plants and various insects). From the analysis
1752 of time-series data in natural and laboratory populations, and from evolutionary theoretical
1753 considerations, several authors have suggested that natural populations likely exhibit periodic and
1754 perhaps chaotic fluctuations (Anderson et al., 2008; Benincà et al., 2008; Edmunds et al., 2003;
1755 Ferriere and Gatto, 1993; Schaffer and Kot, 1986; Tilman and Wedin, 1991), although the subject has
1756 hardly been free from debate (Doebeli and Koella, 1996, 1995; Hassell et al., 1976; Lande et al., 1997).
1757 If endogenous fluctuations are possible, our analysis suggests that the shape (log-concavity) of growth
1758 functions will affect both the moments of a resident species as well as the way in which these moments
1759 are "felt" by an invader. In experimental or observational systems, empirical assessment of the shape
1760 of per capita growth curves in competitive, host-pathogen, and predator-prey systems will help
1761 determine whether such endogenous fluctuations can promote species diversity or even reverse
1762 expected outcomes in nature.
1763

1764 **Appendix A: Proof of the discrete-time competitive exclusion principle**

1765 Suppose that species *k* has the highest equilibrium when alone of *S* competing species in a Volterrian
1766 community. For any $i \neq k$, we define:

1767 $$\Omega_i(t) = \frac{N_i(t)^{1/\beta_i}}{N_k(t)^{1/\beta_k}}$$

1768 By equation (2), it follows that

1769 $$\Omega_i(t+1) = \frac{G_i\big(\mathbf{N}(t)\big)^{1/\beta_i}}{G_k\big(\mathbf{N}(t)\big)^{1/\beta_k}}\Omega_i(t)$$

1770 By condition (3), $G_i\big(\mathbf{N}(t)\big) = exp\{\alpha_i - \beta_i H\big(\mathbf{N}(t)\big)\}$ and we have

1771 $$\Omega_i(t+1) = e^{(\Phi_i - \Phi_k)}\Omega_i(t)$$

where $\Phi_i = \alpha_i/\beta_i$. Letting $\eta_i = e^{(\Phi_i - \Phi_k)}$, we have the following solution for $\Omega_i(t)$:

$$\Omega_i(t) = (\eta_i)^t \Omega_i(0)$$

Since $\Phi_i < \Phi_k$ (see section B.5 of the Supplementary Information), we have $0 < \eta_i < 1$. Thus,

$$\lim_{t\to\infty} \Omega_i(t) = \lim_{t\to\infty} (\eta_i)^t \Omega_i(0) = 0$$

Each species has an upper bound (see section B.2 of the Supplementary Information). Let the upper bound of species *k* be given by $N_k^{\max}$. We must have

$$0 \leq \frac{N_i(t)^{1/\beta_i}}{[N_k^{\max}]^{1/\beta_k}} \leq \frac{N_j(t)^{1/\beta_i}}{N_k(t)^{1/\beta_k}}$$

Since $\lim_{t\to\infty} 0 = 0$ and $\lim_{t\to\infty} \frac{N_j(t)^{1/\beta_i}}{N_k(t)^{1/\beta_k}} = 0$, the squeeze rule for limits guarantees $\lim_{t\to\infty} \frac{N_i(t)^{1/\beta_i}}{[N_k^{\max}]^{1/\beta_k}} = 0$.

Using the scalar rule for limits, it follows that $\lim_{t\to\infty} N_i(t)^{1/\beta_i} = 0$.

Because $\beta_i > 0$ and $N_i(t) > 0$ for all *t*,

$$\lim_{t\to\infty} N_i(t) = 0$$

This means all species other than species *k* go extinct. We now turn to species *k*.

Assume that species *k* also goes extinct, meaning $\lim_{t\to\infty} N_k(t) = 0$. Given that G_k is continuous and $G_k(\vec{\mathbf{0}}) > 1$, there exists some $\varepsilon > 0$, such that if $\|\mathbf{N}\| < \varepsilon$, $G_k(\mathbf{N}) > 1$. If $\lim_{t\to\infty} N_k(t) = 0$, then, at some time point t^*, $\mathbf{N}(t^*)$ will be located closer than ε to the origin and $\mathbf{N}(t)$ will stay closer to the origin than ε for all $t \geq t^*$. However, this means that $N_k(t+1) = G_k(\mathbf{N}(t))N_k(t) > N_k(t)$ for all $t \geq t^*$. Given that $N_k(t^*) > 0$, it cannot then be the case that $\lim_{t\to\infty} N_k(t) = 0$, which contradicts our assumption that species *k* goes extinct. Therefore, we may conclude that species *k* persists and all other species are driven to extinction, which completes the proof of the competitive exclusion principle.

1793 Given some initial condition for a Volterrian community, we now show that it must be contained

1794 within a shifting lower-dimensional subspace. To do this, we define:

1795 $$\Lambda(\mathrm{t}) = \left\{\prod_{i=1}^{S} \frac{N_j(t)^{1/\beta_i}}{N_k(t)^{1/\beta_k}}\right\}^{1/S}$$

1796 By equation (2), we have the following:

1797 $$\Lambda(\mathrm{t}+1) = \left\{\prod_{i=1}^{S} \frac{G_i\big(\mathbf{N}(t)\big)^{1/\beta_i}}{G_k\big(\mathbf{N}(t)\big)^{1/\beta_k}}\right\}^{1/S} \Lambda(\mathrm{t})$$

1798 Following the earlier approach starting from condition (3), this can be rewritten as

1799 $$\Lambda(\mathrm{t}+1) = e^{(\overline{\Phi}-\Phi_k)}\Lambda(\mathrm{t})$$

1800 where $\overline{\Phi} = \frac{1}{S}\sum_{i=1}^{S} \Phi_i$. Iterating gives us the general formula:

1801 $$\Lambda(\mathrm{t}) = \kappa^t \Lambda(0)$$

1802 with $\kappa = e^{(\overline{\Phi}-\Phi_k)}$. Using this relationship, we know that the community must be in a subspace at *t*

1803 satisfying:

1804 $$N_k = (\kappa^{-\omega_k})^t \big(\Lambda(0)\big)^{-\omega_k} \prod_{i \in S_{-k}} N_i^{\omega_k/S\beta_i}$$

1805 where $\omega_k = \beta_k S/(S-1)$ and $\mathbf{S}_{-k}$ is the set of integers from 1 to *S* without *k*. Here we take the density

1806 of species *k* as the dependent variable. In Figure 3 and the Supplementary Information (section B.7) we

1807 show how dynamics (in particular, competitive exclusion) can be visualized using this moving

1808 subspace.

1809

1810 **Appendix B: Derivation of the invasion heuristic for 2-species communities**

1811 Consider two species, labeled 1 and 2. Species 1 will be the resident species. In the absence of species

1812 2, the abundance of species 1 enters a bounded positive interval (given our assumptions about growth

functions; see Supplementary Information, section A.3). Species 2 is the invader and starts at a very low density (such that its initial success is determined by its growth function and the abundance of species 1, but not its own abundance). The population recursion for the invader is given by:

$$N_2(t+1) = G_2\big(N_1(t), N_2(t)\big)N_2(t)$$

If an invader is to increase from very low density, then its long-term per capita growth rate (the relevant Lyapunov number, $\widetilde{G_2}$) must be greater than unity. In other words:

$$\widetilde{G_2} = \lim_{T\to\infty} \sqrt[T]{\prod_{t=0}^{T-1} G_2(N_1(t), 0)} > 1$$

Alternatively, this can be expressed as:

$$\ln \widetilde{G_2} = \lim_{T\to\infty} \left\{ \frac{1}{T} \sum_{t=0}^{T-1} \ln G_2(N_1(t), 0) \right\} > 0$$

Given that the density of species 1 gets trapped in a bounded interval, the mean abundance and variance in abundance of the resident are:

$$\overline{N_1} = \lim_{T\to\infty} \left\{ \frac{1}{T} \sum_{t=0}^{T-1} N_1(t) \right\}$$

$$\sigma_{N_1}^2 = \lim_{T\to\infty} \left\{ \frac{1}{T} \sum_{t=0}^{T-1} (N_1(t) - \overline{N_1})^2 \right\}$$

assuming both limits exist. To estimate $\ln \widetilde{G_2}$, we use a second-order Taylor series approximation of $\ln G_2(N_1(t), 0)$ centered at the mean resident abundance, $\overline{N_1}$:

$$\ln \widetilde{G_2} \approx \lim_{T\to\infty} \frac{1}{T} \sum_{t=0}^{T-1} \left\{ \ln G_2(\overline{N_1}, 0) + (N_1(t) - \overline{N_1}) \frac{d \ln G_2(N_1, 0)}{dN_1}\bigg|_{N_1=\overline{N_1}} \right.$$

$$\left. + \left(\frac{(N_1(t) - \overline{N_1})^2}{2} \right) \frac{d^2 \ln G_2(N_1, 0)}{dN_1{}^2}\bigg|_{N_1=\overline{N_1}} \right\}$$

By using the scalar and additive rules for limits, we have:

$$\ln \widetilde{G_2} \approx \ln G_2(\overline{N_1}, 0) + \left(\lim_{T\to\infty} \frac{1}{T} \sum_{t=0}^{T} N_1(t) \right) \left. \frac{d \ln G_2(N_1, 0)}{dN_1} \right|_{N_1=\overline{N_1}} - \overline{N_1} \left. \frac{d \ln G_2(N_1, 0)}{dN_1} \right|_{N_1=\overline{N_1}}$$

$$+ \left(\lim_{T\to\infty} \frac{1}{T} \sum_{t=0}^{T} (N_1(t) - \overline{N_1})^2 \right) \left(\frac{1}{2}\right) \left. \frac{d^2 \ln G_2(N_1, 0)}{dN_1{}^2} \right|_{N_1=\overline{N_1}}$$

Using the definitions of the mean and variance, we have:

$$\ln \widetilde{G_2} \approx \ln G_2(\overline{N_1}, 0) + \left(\frac{\sigma_{N_1}^2}{2} \right) \left. \frac{d^2 \ln G_2(N_1, 0)}{dN_1{}^2} \right|_{N_1=\overline{N_1}}$$

Or simply

$$\widetilde{G_2} \approx G_2(\overline{N_1}, 0) \exp \left\{ \left(\frac{\sigma_{N_1}^2}{2} \right) \left. \frac{d^2 \ln G_2(N_1, 0)}{dN_1{}^2} \right|_{N_1=\overline{N_1}} \right\}$$

This approximation derives from a second-order Taylor series. If the logarithm of the invader's growth function ($\ln G_2$) is linear or quadratic, then the approximation is exact.

References

Adler, F.R. (1990). Coexistence of two types on a single resource in discrete time. J. Math. Biol. *28*, 695–713.

Anderson, C.N.K., Hsieh, C., Sandin, S.A., Hewitt, R., Hollowed, A., Beddington, J., May, R.M., and Sugihara, G. (2008). Why fishing magnifies fluctuations in fish abundance. Nature *452*, 835–839.

Armstrong, R.A., and McGehee, R. (1980). Competitive Exclusion. The American Naturalist *115*, 151–170.

Asmussen, M.A. (1979). Regular and chaotic cycling in models of ecological genetics. Theoretical Population Biology *16*, 172–190.

Benincà, E., Huisman, J., Heerkloss, R., Jöhnk, K.D., Branco, P., Van Nes, E.H., Scheffer, M., and Ellner, S.P. (2008). Chaos in a long-term experiment with a plankton community. Nature *451*, 822–825.

Chesson, P. (2000). Mechanisms of Maintenance of Species Diversity. Annual Review of Ecology and Systematics *31*, 343–366.

Cushing, J.M., Levarge, S., Chitnis, N., and Henson, S.M. (2004). Some Discrete Competition Models and the Competitive Exclusion Principle†. Journal of Difference Equations and Applications *10*, 1139–1151.

Doebeli, M., and Koella, J. (1996). Chaos and evolution. Trends in Ecology & Evolution *11*, 220.

Doebeli, M., and Koella, J.C. (1995). Evolution of Simple Population Dynamics. Proceedings of the Royal Society of London B: Biological Sciences *260*, 119–125.

Edmunds, J., Cushing, J.M., Costantino, R.F., Henson, S.M., Dennis, B., and Desharnais, R.A. (2003). Park's Tribolium competition experiments: a non-equilibrium species coexistence hypothesis. Journal of Animal Ecology *72*, 703–712.

Ferriere, R., and Gatto, M. (1993). Chaotic Population Dynamics can Result from Natural Selection. Proceedings of the Royal Society of London B: Biological Sciences *251*, 33–38.

Ferriere, R., and Gatto, M. (1995). Lyapunov Exponents and the Mathematics of Invasion in Oscillatory or Chaotic Populations. Theoretical Population Biology *48*, 126–171.

Franke, J.E., and Yakubu, A.-A. (1991). Mutual exclusion versus coexistence for discrete competitive systems. J. Math. Biol. *30*, 161–168.

Gatto, M. (1993). The Evolutionary Optimality of Oscillatory and Chaotic Dynamics in Simple Population Models. Theoretical Population Biology *43*, 310–336.

Gause, G.F. (1934). The Struggle for Existence (Baltimore: Williams and Wilkins).

Hardin, G. (1960). The Competitive Exclusion Principle. Science *131*, 1292–1297.

Hassell, M.P. (1975). Density-Dependence in Single-Species Populations. Journal of Animal Ecology *44*, 283–295.

Hassell, M.P., and Comins, H.N. (1976). Discrete time models for two-species competition. Theoretical Population Biology *9*, 202–221.

Hassell, M.P., Lawton, J.H., and May, R.M. (1976). Patterns of Dynamical Behaviour in Single-Species Populations. Journal of Animal Ecology *45*, 471–486.

Hastings, A., Hom, C.L., Ellner, S., Turchin, P., and Godfray, H.C.J. (1993). Chaos in Ecology: Is Mother Nature a Strange Attractor? Annual Review of Ecology and Systematics *24*, 1–33.

Huisman, J., and Weissing, F.J. (1999). Biodiversity of plankton by species oscillations and chaos. Nature *402*, 407–410.

Lande, R., Sæther, B.-E., and Engen, S. (1997). Threshold Harvesting for Sustainability of Fluctuating Resources. Ecology *78*, 1341–1350.
Leslie, P.H., Park, T., and Mertz, D.B. (1968). The Effect of Varying the Initial Numbers on the Outcome of Competition Between Two Tribolium Species. Journal of Animal Ecology *37*, 9–23.
May, R.M. (1974). Biological Populations with Nonoverlapping Generations: Stable Points, Stable Cycles, and Chaos. Science *186*, 645–647.
May, R.M. (1975). Biological populations obeying difference equations: Stable points, stable cycles, and chaos. Journal of Theoretical Biology *51*, 511–524.
May, R.M., and Oster, G.F. (1976). Bifurcations and Dynamic Complexity in Simple Ecological Models. The American Naturalist *110*, 573–599.
Metz, J.A., Nisbet, R.M., and Geritz, S.A. (1992). How should we define "fitness" for general ecological scenarios? Trends Ecol. Evol. (Amst.) *7*, 198–202.
Nelder, J.A. (1961). The Fitting of a Generalization of the Logistic Curve. Biometrics *17*, 89–110.
Ricker, W.E. (1954). Stock and Recruitment. J Fisheries Research Board of Canada *11*, 559–623.
Schaffer, W.M., and Kot, M. (1986). Chaos in ecological systems: The coals that Newcastle forgot. Trends in Ecology & Evolution *1*, 58–63.
Tilman, D. (1982). Resource Competition and Community Structure (Princeton University Press).
Tilman, D., and Wedin, D. (1991). Oscillations and chaos in the dynamics of a perennial grass. Nature *353*, 653–655.
Vandermeer, J., Evans, M.A., Foster, P., Höök, T., Reiskind, M., and Wund, M. (2002). Increased competition may promote species coexistence. PNAS *99*, 8731–8736.
Volterra, V. (1928). Variations and Fluctuations of the Number of Individuals in Animal Species living together. J. Cons. Int. Explor. Mer *3*, 3–51.